



## Review

## Current advances in imaging spectroscopy and its state-of-the-art applications



Anam Zahra<sup>a,1</sup>, Rizwan Qureshi<sup>b,1</sup>, Muhammad Sajjad<sup>c,1</sup>, Ferhat Sadak<sup>d,e</sup>, Mehmoond Nawaz<sup>f,1</sup>, Haris Ahmad Khan<sup>g,h,\*</sup>, Muhammad Uzair<sup>i</sup>

<sup>a</sup> Max Planck Institute of Evolutionary Anthropology, Germany

<sup>b</sup> Fast School of Computing, National University of Computer and Emerging Sciences, Karachi, Pakistan

<sup>c</sup> Department of Geography and Centre for Geo-computation Studies, Hong Kong Baptist University, Hong Kong Special Administrative Region of China

<sup>d</sup> CNRS, Institut des Systèmes Intelligents et de Robotique, ISIR, Sorbonne Université, 75005 Paris, France

<sup>e</sup> Department of Mechanical Engineering, Bartın University, Bartın, 74100, Turkey

<sup>f</sup> Department of Biomedical Engineering, The Chinese University of Hong Kong, Hong Kong

<sup>g</sup> Agricultural Biosystems Engineering, Wageningen University & Research, Wageningen, The Netherlands

<sup>h</sup> Data Science CDP EAME, Syngenta, The Netherlands

<sup>i</sup> University of Adelaide, Australia

## ARTICLE INFO

## Keywords:

Imaging spectroscopy  
Hyperspectral imaging  
Image processing  
Computer vision  
Remote sensing  
Deep learning

## ABSTRACT

Imaging spectroscopy integrates traditional computer vision and spectroscopy into a single system and has gained widespread acceptance as a non-destructive scientific instrument for a wide range of applications. The current state of imaging spectroscopy spans diverse applications including but not limited to air-borne and ground-based computer vision systems. This paper presents the current state of research and industrial applications including precision agriculture, material classification, medical science, forensic science, face recognition and document image analysis, environment monitoring, and remote sensing, which can be aided through imaging spectroscopy. In this regard, we further discuss a comprehensive list of applications of imaging spectroscopy, pre-processing techniques, and spectral image acquisition systems. Likewise, publicly available databases and current software tools for spectral data analysis are also documented in this review. This review paper, therefore, could potentially serve as a reference and roadmap for people looking for literature, databases, applications, and tools to undertake additional research in imaging spectroscopy.

## 1. Introduction

The electromagnetic spectrum encompasses a broad range of electromagnetic radiation, each characterized by distinct wavelengths and frequencies (Zwinkels, 2015). These include, among others, ultraviolet, visible, infrared, microwaves, and radio waves, each characterized by unique electromagnetic properties such as energy levels, propagation characteristics, and interactions with matter, making them essential subjects of study across various scientific disciplines (Someda, 2017; Weinstein, 1988).

Visible light is an electromagnetic radiation perceptible to the human eye and constitutes a narrow bandwidth within the electromagnetic spectrum, specifically spanning wavelengths between 380 and 780 nanometers (Reinhard et al., 2010). This specific spectral range

forms the basis for numerous well-established techniques and applications in the field of traditional vision and imaging processing (Gonzalez, 2018).

Current advancements in sensor technology have enabled the acquisition of images across a wide range of electromagnetic wavelengths (ElMasry & Sun, 2010b). These include both multi-spectral and hyperspectral images, which encompass more than the traditional three spectral bands used in visible spectrum imaging. Multi-spectral imaging (MSI) and hyperspectral imaging (HSI) techniques involve capturing multiple images at narrow and contiguous spectral bands spanning a wider range of the electromagnetic spectrum, thereby providing an enhanced level of spectral detail. These advanced imaging methods are collectively referred to as imaging spectroscopy.

\* Corresponding author at: Agricultural Biosystems Engineering, Wageningen University & Research, Wageningen, The Netherlands.

E-mail addresses: [anam\\_zahra@eva.mpg.de](mailto:anam_zahra@eva.mpg.de) (A. Zahra), [rizwan.qureshi@nu.edu.pk](mailto:rizwan.qureshi@nu.edu.pk) (R. Qureshi), [msajjad@hkbu.edu.hk](mailto:msajjad@hkbu.edu.hk) (M. Sajjad), [fsadak@bartin.edu.tr](mailto:fsadak@bartin.edu.tr) (F. Sadak), [mehmoondnawaz@cuhk.edu.hk](mailto:mehmoondnawaz@cuhk.edu.hk) (M. Nawaz), [haris.khan@wur.nl](mailto:haris.khan@wur.nl) (H.A. Khan), [muhammad.uzair@adelaide.edu.au](mailto:muhammad.uzair@adelaide.edu.au) (M. Uzair).

<sup>1</sup> Equal Contribution.

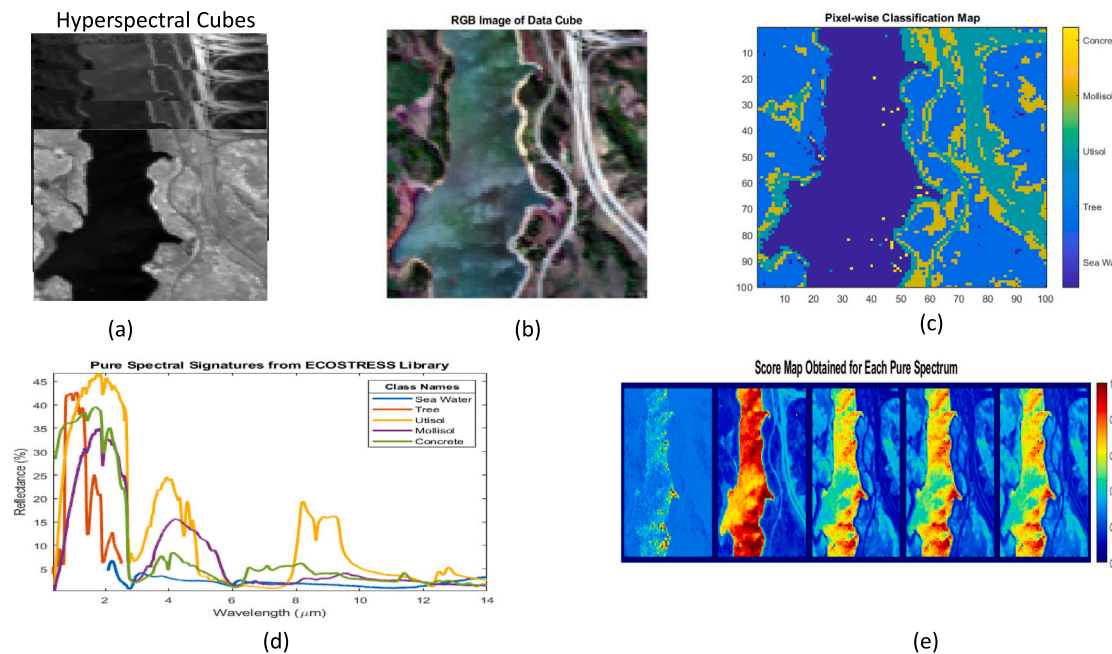


**Fig. 1.** Visualization of Hyperspectral cubes at different wavelengths (a), RGB Image of the hyperspectral cube (b), Pixel-wise classification map, Pure spectral signature of different objects (d), Score map obtained for each pure spectrum. The images are generated using the hyperspectral toolbox of MATLAB 2021 (a). The source image is Jasper Ridge, captured via the airborne visible/infrared imaging spectrometer (AVIRIS). The data set contains areas of water, land, road, and vegetation.

Objects in the natural environment exhibit distinct spectral responses when interacting with electromagnetic radiation (Heald & Marion, 2012). These responses encompass the absorption, transmission, and reflection of electromagnetic radiation, giving rise to unique spectral signatures for various elements and object materials (Khan, Thomas, Hardeberg, & Laligant, 2019). Consequently, imaging spectroscopy enables comprehensive spectral analysis for a wide range of applications in a diverse range of fields including remote sensing (Arelano, Tansey, Balzter, & Boyd, 2015), precision agriculture (Ravikanth, Jayas, White, Fields, & Sun, 2017), chemistry (Cheng, Sun, Pu, & Zhu, 2015), medicine (Lu & Fei, 2014), process monitoring (Pan, Chyngyz, Sun, Paliwal, & Pu, 2019), environmental applications (Bourguignon, Mary, & Slezak, 2010; Zhou & Camba, 2021), military (Shimoni, Haelterman, & Perneel, 2019), food industry (ElMasry, Barbin, Sun, & Allen, 2012; Lorente et al., 2012) and other commercial applications (Xing et al., 2019). It is estimated that the global HSI systems market is expected to grow from USD 15.4 billion in 2021 to USD 35.8 billion by 2026 Wood. The major market segments include; military surveillance, remote sensing, machine vision & optical sorting, life sciences & medical diagnostics, and other applications.

A spectral image is usually in the form of a cube, where the first two dimensions represent the spatial information and the third dimension represents a series of spectral images captured at different wavelengths. For example, a hyperspectral image contains abundant spectral data captured at hundreds of distinct wavelengths across the electromagnetic spectrum, while a multispectral image comprises images captured at several tens of wavelengths. The number of wavelengths/spectral channels in a spectral image usually depends upon the application and the type of instrument. To process this high-dimensional data effectively, many image processing and machine learning pipelines have been developed in the literature, ranging from pre-processing (Vidal & Amigo, 2012), calibration (Behmann et al., 2015) noise modeling (Acito, Diani, & Corsini, 2011), dimensionality reduction (Huang, Shi, He, Duan, & Luo, 2019), anomaly detection (Zhang, Wen, & Dai, 2016), clustering (Zeng, Cai, Liu, Cai, & Li, 2019), spectral unmixing (Bendoumi, He, & Mei, 2014), feature extraction (Kumar, Dikshit, Gupta, & Singh, 2020), representation learning (Sellami & Tabbone,

2022), classification (Yusuf & Alawneh, 2018) and regression, tailored specifically to imaging spectroscopy (Minasny & McBratney, 2008).

In imaging spectroscopy, especially in HSI, the spectrum for each pixel is measured at different wavelengths as shown in Fig. 1. In order to provide more information on what is imaged, the radiation striking each pixel is broken down into many different spectral bands (Armin Schneider, 2017). Fig. 1(a) presents a hyperspectral cube and each slice of the cube represents images captured at different wavelengths, Fig. 1(b) presents a color image from the hyperspectral cube, and part (c) presents a pixel-wise classification map. The original image is from the hyperspectral dataset Jasper Ridge, captured using AVIRIS (Green et al., 1998) air-borne spectrometer (Kruse et al., 1993). Part (d) and (e) of Fig. 1 show the unique spectral signature and spectrum score of each entity respectively. The spectrum score is computed by measuring the degree of similarities between spectra using the Spectral Angle Mapper (SAM) classification algorithm (Kruse et al., 1993). Imaging spectrometers typically operate in the 0.4 to 2.5  $\mu\text{m}$  wavelength range, capturing the visible and solar-reflected infrared spectrum (i.e., near-infrared or NIR, and short-wavelength infrared or SWIR) from the observed materials (Paoletti, Haut, Plaza, & Plaza, 2019). While hyperspectral sensors have been predominantly utilized in satellite applications, narrow-band hyperspectral sensors have also explored for ground-based computer vision systems, such as face recognition (Qureshi, Uzair, & Zahra, 2020; Uzair, Mahmood, & Mian, 2015), document image analysis (Qureshi, Uzair, Khurshid, & Yan, 2019), ink-mismatch detection (Khan, Shafait, & Mian, 2013), forgery detection (Khan, Yousaf, Abbas, & Khurshid, 2018), and non-destructive forensic analysis of classified documents (Khan, Khan, Yousaf, Khurshid, & Khan et al. Abbas, 2018).

Given the emergence of this field in the past decade, many researchers have provided reviews on imaging spectroscopy. For example, the use of HSI imaging in forensic science is presented in Melit Devassy and George (2021), document image analysis in Qureshi et al. (2019), skin diseases in Chen et al. (2020), cancer cell segmentation in Alouogianni et al. (2022), deep learning methods for agriculture in Fadhlallah Guerri, Distante, Spagnolo, Bougourzi, and Taleb-Ahmed (2023), spectral reconstruction methods from RGB image in Zhang et al. (2022), and a survey on applications of HSI is presented

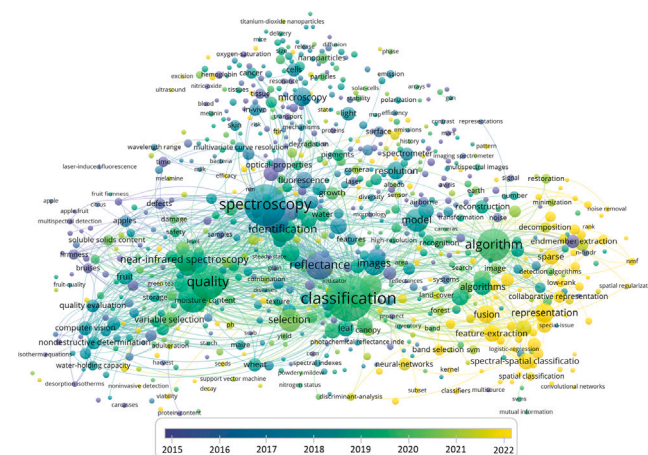


**Fig. 2.** Terms co-occurrence in Hyperspectral publications during 2015–2022. During 2015–2022, several distinct clusters could be seen including the largest occurrence of reflectance, spectroscopy, classification, quality, algorithm, and feature extraction (listed chronologically).

in Khan, Khan, et al. (2018). The medical applications of HSI are discussed in Fei (2019), Karim, Qadir, Farooq, Shakir, and Laghari (2023), Lu and Fei (2014), and food and safety applications of HSI are discussed in Feng and Sun (2012). The use of machine learning and deep learning for hyperspectral image classification is presented in Datta et al. (2022).

While earlier reviews have provided valuable insights, the field of imaging spectroscopy has experienced significant advancements in recent years. For example, there has been substantial and rapid progress in HSI imaging technology. Similarly, the availability of new HSI datasets, and their usage in new applications, as shown in Figs. 2 and 3. Fig. 2 illustrates that the research landscape and trends in the field of HSI during 2015–2022 have rapidly evolved. In terms of source comparison (i.e., platforms publishing HSI-related research), IEEE and ScienceDirect are leading the HSI-related research production with larger impact and visibility (Fig. 3).

Since the field is continuously evolving at a faster pace, it is important to review the recent advancements, developments, and challenges to reflect the state of the field. Thus, a comprehensive review of the recent advancements in terms of applications, databases, software, and future prospects could progressively benefit the community. In connection with this, we present an updated comprehensive review of the state of HSI and its state-of-the-art applications across various scientific and professional fields. Such a review could potentially act as a roadmap and would progressively provide useful references to research and the professional community in terms of literature, databases, tools, and applications of imaging spectroscopy.

The rest of the paper is organized as follows. We first discuss imaging spectroscopy acquisition systems with camera models and lens specifications. Within the spectroscopy, our focus is mainly on HSI. This is followed by the discussion on pre-processing challenges and methods for processing hyperspectral images, including spikes removal, dead pixels, compression, and spectral processing in Section 3. Applications of HSI in modern-day societies, such as medicine, precision agriculture, remote sensing, food quality control, material classification, document image analysis, and face recognition are discussed in Section 4. Next, we present open-source hyper-spectral databases and software libraries for processing hyperspectral images in Section 5. Finally, Section 6 summarizes the key insights from this study. A list of acronyms used in the paper is given in Table 1.

**Table 1**  
List of acronyms used in the paper.

Acronyms	Definition
CCD	Charge-coupled device
CMOS	Complementary metal oxide semiconductor
HSI	Hyperspectral imaging
MSI	Multispectral imaging
LAI	Leaf area index
LCTF	Liquid crystal tuneable filter
UAV	Unmanned aerial vehicle
PCA	Principal component analysis
ICA	Independent component analysis
PSLR	Partial least square regression
SAM	Spectral angle mapper
MSC	Multiplicative scatter correction
CNN	Convolutional neural network
GNN	Graph neural network
NASA	National Aeronautics and Space Administration

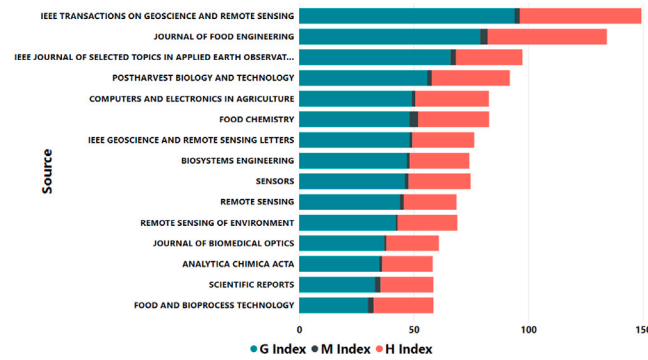


**Fig. 3.** Publications related to imaging spectroscopy across various peer-reviewed journals. IEEE Transactions on Geosciences and Remote Sensing from the IEEE platform is the most prominent source with the largest G-Index and H index followed by the Journal of Food Engineering from the ScienceDirect platform. Considering the specialized nature of these journals, geosciences and food engineering fields are the ones where the most prominent applications of HSI might be seen.

## 2. Acquisition of hyperspectral images

Spectral sensors are used to collect data in the form of images, where each image represents a specific wavelength range of the electromagnetic spectrum known as a spectral band. These images are combined to create a three-dimensional hyperspectral data cube for further processing and analysis. The cube consists of two spatial dimensions ( $x$  and  $y$ ) and a spectral dimension  $\lambda$  comprising a range of wavelengths (Khan, Thomas, Hardeberg, & Laligant, 2017).

There are different modes of operation for acquiring spectral data, each with its own advantages and disadvantages. One such technique is the Whiskbroom method, which involves mounting a linear array of detectors on a moving platform, such as an aircraft or satellite, and pointing it towards the ground. As the platform moves forward, the detectors collect data from a narrow strip of the ground, known as a swath. The collected data is used to create an image of the scene, with each pixel containing spectral information.

Another method is the pushbroom method, which involves line scanning across a single axis, and an image is created by either moving the camera or the objects of interest. The movement should be consistent to avoid spatial distortions in the acquired data. Plane scanning is another method for acquiring spectral data, where the entire region is scanned at different wavelength intervals. This can be done using a liquid crystal tuneable filter (LCTF) that allows a particular wavelength bandwidth at a time. The resultant images are embedded on top of each other to acquire spectral data.

A recent development in imaging spectroscopy is the integration of thin-film spectral filters on top of the image sensor. This eliminates

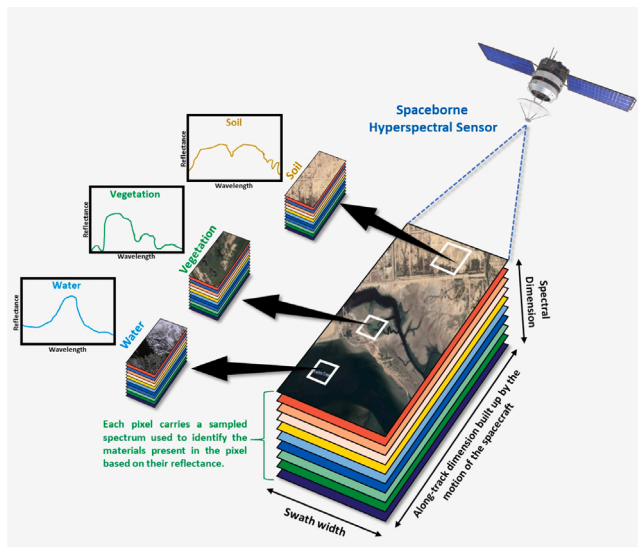


**Fig. 4.** An example of HSI imaging in mapping soil, vegetation, and water. Source: The figure is modified from Khan, Khan, et al. (2018).

the need for complex optical systems and moving hardware systems, allowing for rapid data acquisition and use in video mode without requiring a stationary scene.

During data acquisition, it is crucial to ensure the presence of a consistent light source and calibration tiles. Any change in illumination can affect the acquired data, which can have an impact on the further processing of the imaging spectroscopy data (Khan, Thomas, Hardeberg, & Laligant, 2018). Methods have been developed for illuminant invariant representation of images in uncontrolled imaging conditions (Khan, 2018; Khan, Thomas, & Hardeberg, 2017, 2018; Khan, Thomas, Hardeberg, & Laligant, 2017).

Overall, the acquisition of spectral data involves various techniques and considerations, and selecting the appropriate method depends on the specific requirements of the application.

### 2.1. Air-borne hyperspectral sensors

Fig. 4 shows a hyperspectral image captured by an air-borne satellite sensor. Existing HSI devices can acquire 3D  $xy\lambda$  volumes using 2D sensors  $ij$  by transforming the spectral dimension in time or arranging it in space. The precision of these sensors is often assessed in terms of spectral resolution, which is the breadth of each collected band of the spectrum. It is possible to identify objects even if they are only captured in a handful of pixels, provided the scanner identifies a large number of reasonably small frequency bands.

#### 2.1.1. Spatial scanning

Spatial resolution can be defined as the smallest detail in an image, which determines the clarity of the image (Gonzalez, 2009). In spatial scanning, each two-dimensional (2-D) sensor output represents the entire slit spectrum. Slit spectra are obtained by projecting a strip of the scene onto a slit and dispersing the slit image with a prism or grating in spatial scanning HSI systems. Generally speaking, spatial resolution shows the size of the pixel, whereas spectral resolution shows the content of the pixel in an image.

#### 2.1.2. Spectral scanning

A single pixel's spectrum in a hyperspectral image can reveal significantly more information about the material's surface than in a regular image. Another acquisition approach that requires the incoming images to be filtered to produce a  $xyk$  image at time  $tk$  is spectral acquisition

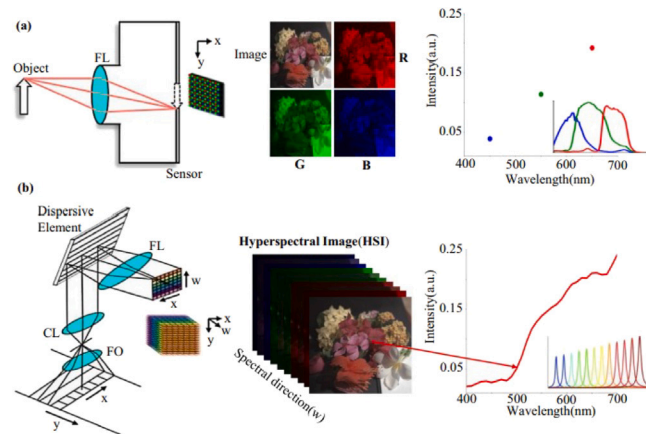


**Fig. 5.** Schematic diagrams of an RGB camera (a) and a typical hyperspectral imager (b). Each pixel in an RGB image combines three distinct color values that are integrated from the R, G, and B spectra. Each pixel in a hyperspectral image is a continuous spectral curve formed from a number of tiny spectral bands. FO front objective, CL collimating lens group, and FL focusing lens group. The images are from the KAUST-HS open-source dataset (Li, Fu, & Heidrich, 2021). Source: Figure adopted from Zhang et al. (2022).

in time. Each 2-D sensor output in spectral scanning represents a monochromatic ('single-colored') spatial ( $x, y$ ) map of the scene. HSI spectrum scanning devices are typically based on optical band-pass filters (either tuneable or fixed). The scene is spectrally scanned by switching between filters while the platform remains steady.

#### 2.1.3. Temporal scanning

Temporal resolution is defined as the amount of time needed to revisit and acquire data for the exact same location by the hyperspectral sensor (Ma et al., 2021). The fundamental trade-off here is between spectral and temporal resolution, with spectral filtering performed through mechanical filter wheels (usually restricted to MSI) or acousto-optical or liquid-crystal tuneable filters (enabling HSI at a higher cost). The ability to obtain a spectrum image by simply taking a snapshot is very appealing for time-constrained applications, and this has sparked a lot of study (Hagen & Kudinov, 2013).

#### 2.1.4. Spatio-spectral scanning

In spatio-spectral scanning, each 2-D sensor output represents a wavelength-coded ('rainbow-colored', =  $(y)$ ), spatial ( $x, y$ ) representation of the scene. A camera at some non-zero distance behind a simple slit spectroscope (slit + dispersive element) is used as a prototype for this technology, which was introduced in 2014 (Grusche, 2014).

### 2.2. Ground-based hyperspectral systems

Imaging spectroscopy is a versatile technology that finds applications in various fields such as medical, forensic image analysis, agriculture, and material classification. In ground-based applications, a hyperspectral imaging system typically comprises a light source, a charge-coupled device (CCD) or complementary metal oxide semiconductor (CMOS) camera, and a spectrograph.

Fig. 5 shows a typical ground-based hyperspectral imaging system. The system collects data over a range of wavelengths, typically spanning from the visible to the near-infrared region of the electromagnetic spectrum. The resulting hyperspectral data cube can be analyzed using various techniques, such as spectral unmixing, classification, and feature extraction, to extract valuable information about the scene or object being imaged.

Recently, there has been growing interest in using deep learning algorithms to build hyperspectral images from RGB photos or other

**Table 2**

Pre-processing challenges of HSIs.

Pre-processing challenges	Algorithms	Advantages	Drawbacks
Spikes Removal	Thresholding, Outlier detection or smoothing methods	Robust and reliable	Time-consuming
Dead pixels	Manual Inspection, Heuristic Algorithms	Robust, and reliable	Hyper-parameter optimization
Spectral pre-processing	Multiplicative Scatter Correction (Dhanoa, Lister, Sanderson, & Barnes, 1994), Statistical methods	Easy implementation	Not Robust
Compression	Factor models, Heuristic methods	Easy implementation	loss of spectral details
Background removal	Threshold, salient region detection	Easy implementation	Not Robust
Image Enhancement	Salient Region, Super-pixel	Carry more information	Not Robust

sparse spectral representations (Xiong et al., 2017). This approach has the potential to reduce the cost and complexity of HSI systems and make them more accessible to a wider range of applications.

### 3. Pre-processing of hyperspectral images and data analysis methods

Imaging spectroscopy often results in a multi-dimensional and massive amount of data, which requires extensive pre-processing before useful information extraction and analysis. In this section, we discuss some pre-processing challenges and data analysis algorithms for HS images. Hyperspectral data analysis typically involves several pre-processing steps to correct for various sources of noise and artifacts, such as radiometric calibration, atmospheric correction, and noise reduction.

#### 3.1. Pre-processing challenges and methods for hyperspectral images

The majority of HSI cameras are spectroscopic instruments. As a result, they, like all spectrometers, must be calibrated in order to receive reliable spectral information. Table 2 presents common pre-processing challenges and methods to deal with them.

##### 3.1.1. Calibration of hyperspectral images

Calibration of hyperspectral images is an essential step in the processing and analysis of hyperspectral data to ensure accurate and reliable results (Geladi, Burger, & Lestander, 2004). The goal of calibration is to correct for errors in the radiometric (Wyatt, 2012) and spectral response (Guanter, Richter, & Moreno, 2006) of the sensor. Radiometric calibration is usually done by using a calibrated reference target, such as a white tile or a blackbody, and spectral calibration is done by using a set of known spectral radiance standards.

In addition to radiometric and spectral calibration, there are a number of other calibration methods that can be used for hyperspectral images, including geometric calibration (de Oliveira, Tommaselli, & Honkavaara, 2016), atmospheric calibration (Jia et al., 2020), and radiometric normalization (Chen et al., 2023). The choice of which calibration methods to use will depend on the specific application of the hyperspectral images (Sagan et al., 2021).

##### 3.1.2. Data enhancement, super resolution, and fusion

The physical limitations of hyperspectral sensors may compromise the quality of acquired hyperspectral images. Image enhancement methods like super-resolution can be a good choice to improve the quality of hyperspectral data (Farsiu, Robinson, Elad, & Milanfar, 2004). High-resolution hyperspectral pictures are generated from lower-resolution HSI data by utilizing high spatial-resolution information from another imaging source.

##### 3.1.3. Spikes

Spikes are a sudden rise or a fall in pixel values, that may be generated due to instrument malfunction, environment, or imperfection in electronic circuitry. They often mask the detail in an image and lead to inaccurate analysis. One way to deal with spikes is manual supervision, which requires human attention and is time-consuming. Hyperspectral data contain a massive amount of information, so inspecting them manually is a tedious task. Interpolation, smoothing, or

removing spikes based on the neighboring pixel (Behrend, Tarnowski, & Morris, 2002; Zhang & Henson, 2007) is also good choices. Other options for spike identification include density distribution, median and median modified Wiener filters. Cannistraci, Monteverchi, and Alessio (2009).

##### 3.1.4. Dead pixels

Another issue in HSI is the presence of dead pixels, caused by the sampling error in the detector. These are usually replaced by average, zeros, or the maximum value. The location and amount of dead pixels vary depending on whether they are in a single pixel, a group of pixels, or a whole pixel line. Thresholding can be a good choice to locate dead pixels. The heuristic algorithms, such as swarm optimization (Kennedy & Eberhart, 1995), genetic algorithms can also produce better results. Spectral derivatives can be used to remove additive and multiplicative effects in spectra (Tsai & Philpot, 1998).

##### 3.1.5. Spectral preprocessing

Spectral pre-processing is essential to eliminate unwanted phenomena such as light scattering, particle size effects, and morphological differences impacting spectral measurement. Multiplicative Scatter Correction (MSC) (Dhanoa et al., 1994) and Standard Normal Variate (SNV) are widely used in spectral pre-processing.

##### 3.1.6. Image size and compression

An HS image consists of a series of spectral images captured at different wavelengths, thus image size is larger than the normal RGB images. For example, a  $512 \times 512$  HS image with 200 bands contains more than 52 million data points. To process HSI images, a large amount of memory, transmission speed, and efficient processing pipelines are required. In many cases, image compression techniques are employed, such as byte encoding and data binning. The redundant spectral information can be removed by using Heuristic algorithms, such as Genetic algorithm, Ant colony optimization, and swarm optimization (Leardi, 2001). Factor model approaches like principle component analysis and multivariate curve analysis can be used to significantly reduce the spectral dimension. Partial least square regression (PLSR) or spectral unmixing can be used to select the most informative spectral bands (Sun & Du, 2019).

##### 3.1.7. Background removal

To efficiently process HS images, background removal is used. The non-informative background or outliers in the dataset, caused by the instrument error or radiation, complicates the processing. To clean up and extract the relevant information from the hyperspectral cube, traditional image pre-processing techniques such as histogram detection to detect sharp changes in an image or manual selection of a threshold value can be used Nawaz and Yan (2020a), Khan, Nawaz, Guoxia, and Yan (2019), and Saeed, Murad, Nawaz, and Irum (2017).

### 3.2. Feature extraction

To identify and extract meaningful information from the high dimensional complex HSI data, feature extraction techniques may be use-

ful, which can then be used for a variety of applications such as target detection, classification, and mapping. Principal Component Analysis (PCA), Independent Component Analysis (ICA), and Spectral Angle Mapper (SAM) are some popular feature extraction methods Nawaz, Qureshi, Tivevo, and Shahid (2022), Nawaz and Yan (2020b).

Hong, Wu, et al. (2020) proposed a novel method for extracting spatially semantic information from hyperspectral images. The proposed method (Hong, Wu, et al., 2020) is divided into two parts: feature extraction and classification. Invariant attribute profile IAPs are extracted from the hyperspectral image during the feature extraction step. IAPs are spatial and frequency domain features that capture both spectral and spatial information. They are designed to be insensitive to rotation, translation, and scale changes, making them resistant to image variations. The IAP method extracts feature vectors from hyperspectral images by first computing the spatial gradient and Fourier transform of the spectral signature of each pixel. The gradient and Fourier components are then combined to form a joint feature vector, which is then used to extract invariant attribute profiles using a Gaussian mixture model. These profiles capture both fine and coarse details of the underlying material or object by representing the spatial-frequency information of the pixel's spectral signature.

### 3.2.1. Feature selection

Feature selection techniques aim to identify the most informative spectral bands that capture the target material's essential spectral signature while discarding redundant or irrelevant spectral bands (Ghosh, Datta, & Ghosh, 2013). Minimum redundancy maximum relevance (mRMR) (Kamandar & Ghassemian, 2011) and recursive feature elimination are two common feature selection techniques for hyperspectral data analysis (RFE) (Kaya, Torun, & Küçük, 2014; Nawaz, Khan, Qureshi, & Yan, 2019). These techniques can help to improve classification accuracy, reduce computational complexity, and improve the results' interpretability.

## 3.3. Classification algorithms

Classification algorithms are an important part of hyperspectral data analysis because they aim to classify or categorize each pixel in the hyperspectral image based on its spectral signature.

### 3.3.1. Unsupervised learning

When the number of classes or categories is not known in advance or when the user wants to explore the data and find natural groupings or patterns, unsupervised classification algorithms can be helpful. For the analysis of hyperspectral data, two popular unsupervised classification algorithms are k-means clustering and hierarchical clustering (Murphy & Maggioni, 2018). The choice of classification algorithm depends on the particular application and the user's objectives.

### 3.3.2. Supervised learning

Supervised learning requires labeled training data, the algorithm then learns the spectral characteristics of each class and assigns new pixels to the most similar class based on their spectral similarity. Common supervised classification algorithms for hyperspectral data analysis include support vector machines (SVMs), random forests, and neural networks (Tang, Liu, Wei, & Tang, 2020).

### 3.3.3. Semi-supervised learning for hyperspectral imaging

Due to the high cost and difficulty of obtaining labeled data, semi-supervised learning has been widely used in hyperspectral imaging. Semi-supervised learning algorithms in this context use both labeled and unlabeled data to learn more robust and discriminative representations of hyperspectral data. The labeled data is used to train a classifier or perform dimensionality reduction in semi-supervised learning for hyperspectral imaging (He, Liu, Wang, & Hu, 2017). The unlabeled data is then used to improve the algorithm's performance by incorporating it

into the learning process. This is typically accomplished by incorporating a regularization term that encourages the learned representation to be smooth and coherent across the data, with the underlying structure of the data expected to align.

### 3.3.4. Graph-based semi-supervised learning

Graph-based methods have been widely used in hyperspectral imaging for various tasks such as classification, segmentation, and anomaly detection. Semi-supervised learning methods based on graphs have shown promising results for processing hyperspectral data. In graph-based methods, a graph is used to represent the relationships between pixels or spectral bands in the data. These methods can propagate labels or information from labeled data to unlabeled data on the graph, and then optimize the learned representation to be consistent with the propagated information.

In Hong, Gao, et al. (2020), authors proposed Graph Convolution Networks (GCNs) to classify hyperspectral images. GCNs are a type of neural network that can operate directly on graphs, which makes them well-suited for working with hyperspectral data, as each pixel in a hyperspectral image can be represented as a node in a graph. The proposed method is divided into two major steps. First, the hyperspectral image is used to create a graph in which each pixel is represented as a node and the edges are defined based on the spatial proximity of the pixels. Second, on the graph, a GCN is trained to classify the image. Overall, the paper presents a novel and effective approach for classifying hyperspectral images using GCNs, which has the potential to improve the accuracy and efficiency of this important application.

In Hong, Yokoya, Chanussot, Xu, and Zhu (2019), a novel framework for dimensionality reduction of hyperspectral images using semi-supervised learning was proposed. The proposed framework entails creating a graph to represent the relationships between the pixels in the hyperspectral image and learning a low-dimensional representation of the data using a multitask regression approach. The framework makes use of both labeled and unlabeled data to learn a discriminative feature representation that preserves semantic information in hyperspectral images.

### 3.3.5. Semi-active learning for hyperspectral imaging

Semi-active learning (Li, Wang, & Tang, 2013) is a subset of semi-supervised learning that entails iteratively selecting the most informative samples from unlabeled data for expert labeling. The goal of semi-active learning is to reduce the amount of labeling required to achieve a given level of performance. Semi-active learning algorithms typically employ a query strategy in order to select the most informative samples based on some measure of uncertainty or diversity.

Ref. (Yao et al., 2022), trained a CNN on a small set of labeled data, and then used the CNN to identify the most informative unlabeled samples for expert labeling. The selected samples are then labeled by the expert, and the CNN is retrained using the newly labeled data. This process is repeated iteratively to improve CNN's performance incrementally.

## 4. Applications of imaging spectroscopy

Imaging spectroscopy has many industrial and research applications across a variety of fields. Imaging spectroscopy is currently used in pharmaceutical, food processing, color measurement, forensic science, and agriculture industries (Lodhi, Chakravarty, & Mitra, 2019). This Section presents the application of imaging spectroscopy in air-borne systems as well as ground-based computer vision applications.

### 4.1. Ground-based applications

Optical devices such as bandpass spectral filters, image sensors, and lenses are commonly used in the construction of ground-based hyperspectral image acquisition systems. The filters are electronically controlled, and the pass band can be modified at a high rate. Ground-based HSI systems are applied in a variety of application areas.

#### 4.1.1. Document image analysis

Forensic examination of document image analysis is also an exciting venue for imaging spectroscopy. The conventional document imaging system uses pattern recognition techniques for three-channel RGB images. Several important applications of document imaging can benefit from imaging spectroscopy; such as signature segmentation, writer identification, forgery detection, and historical document image analysis. A comprehensive review of hyperspectral document image analysis is given in Qureshi et al. (2019). Visualizing the spectrum bands at different wavelengths may provide useful insights into challenging document image analysis problems. In addition, combining the discriminative spectral signature with deep neural networks can pave the way for further studies. Deep neural networks require a huge amount of data, however available hyperspectral datasets consist of only a few samples. To address this issue, domain adaptation, data augmentation, or other generative adversarial networks can be employed to generate synthetic document samples for model training.

#### 4.1.2. Material classification

Hyperspectral machine vision recognizes subtle color changes more correctly and reliably distinguishes distinct materials. For a quality inspection or condition assessment of material/product surfaces, imaging spectroscopy can be utilized as a quick and non-contact method. The autonomous detection of corrosion and determining the status of coatings are two examples of probable use cases (Nawaz, Khan, Cao, Qureshi, & Yan, 2019).

Several researchers have used portable spectrometers to collect real-time data on construction materials. In Illehag et al. (2017), a FieldSpec field spectrometer that could measure the visible, near-infrared (NIR), and shortwave infrared (SWIR) spectrums was employed. The five primary facade materials utilized to identify are glass, concrete, metal, wood, and fiber cement, using the Support Vector Machine and Random Forest algorithms. Manich et al. (2016) conducted a similar study in which they investigated stone and mortar using hyperspectral imaging. The images were captured using a Hamamatsu ORCA-05G camera in conjunction with a Specim V10E imaging spectrograph fitted with a VIS-NIR (400–1000 nm) lens. Their study focused primarily on a thorough evaluation of these materials, as well as the occurrence of fractures, crusting, erosion, exfoliation, and swelling on the façade of the Glasgow Cathedral. The study's findings proved that the combination of a camera and spectrograph, resulting in the development of hyperspectral images, provided a significantly more effective methodology for the evaluation of facade materials when compared to standard surveying procedures. In a wider context, hyperspectral technology has proven to be effective in a variety of material classification applications.

#### 4.1.3. Food quality assessment

Hyperspectral imaging can also be used to acquire images of food products with hundreds of contiguous spectral bands, which may identify and quantify different constituents of the food (Sun, 2010). By measuring the reflectance at different wavelengths, it can be used for grading of fruits and vegetables (Steinbrenner, Posch, & Leitner, 2019), assessment of food quality (ElMasry & Sun, 2010a), packaging and control (Medus, Saban, Francés-Villora, Bataller-Mompeán, & Rosado-Muñoz, 2021).

#### 4.1.4. Art restoration

Imaging spectroscopy is a powerful tool that can be used to improve the understanding and restoration of artworks (Liu et al., 2022). It can be used for a variety of artwork applications, for example, it can identify pigments (Grabowski, Masarczyk, Glomb, & Mendys, 2018), by comparing the spectral signature of the artwork to the known pigments. It can also be used for knowing the distribution of pigments, which may help in identifying paint loss, restoration, or over-painting. Changes in the spectral signature may also help in estimating the degradation process, such as cracking, fading, and yellowing (Vanmeert et al., 2019).

#### 4.1.5. Medical applications

Medical diagnostics and image-guided surgery have both benefited from the employment of HSI. Medical applications can be divided into two main sections: disease diagnosis and surgical guidance.

##### Disease diagnosis

HSI has been used in several studies for medical diagnosis due to its capacity to identify metabolic alterations that occur as a disease develops, such as cancer cell metabolism (Joseph, 2012). This section uses the HSI systems to explore various diseases such as cancers, retinal diseases, and diabetic foot.

##### Cancers

HSI measures the absorption, fluorescence emission, or reflectance spectrum of tissues to detect cancers. The richer spectral information can be exploited to understand the shape of a cancer tumor, as well as its microenvironment. Optical spectroscopy was utilized to identify neoplasia and discovered that increased metabolic activity impacts mitochondrial fluorophores, altering fluorescence characteristics in precancerous tissue (Sokolov, Follen, & Richards-Kortum, 2002), fluorescence and reflectance spectra provide helpful in vivo data and real-time for pre-cancer diagnosis by providing nuclear diameter or refractive index.

*Cervical cancer*, the fourth most frequent cancer among women in 2018, with an estimated 570,000 cases and 311,000 deaths, is currently diagnosed via a pap smear test, which can detect precancerous changes in cervical cells and tissue (Koss, 1989). Ferris et al. (2001) investigated the capacity of Multi-modal imaging spectroscopy (MHI) to detect, locate, and diagnose cervical neoplasia without invasive. Wang et al. (2016) tried to explore the viability and efficacy of multi-scale imaging spectroscopy in identifying cervical neoplasia at tissue and cellular levels. Imaging spectroscopy analysis was shown to be consistent with a histopathological examination, demonstrating the technological viability of multi-scale imaging spectroscopy for cervical neoplasia diagnosis with accuracy and efficacy. Another proof of principle is the use of HSI in prescreening liquid-based Pap test slides to improve Pap test diagnosis by recognizing between normal, precancerous, and cancerous cell (Siddiqi et al., 2008).

*Breast cancer* is another type of widely known cancer, and its early-stage diagnosis is crucial. The optical characteristics of ex-vivo breast tissues alter, resulting in variable reactions to light transmission, absorption, and reflection across the spectrum. Ex-vivo breast cancer was detected using imaging spectroscopy (Aboughaleb, Aref, & El-Sharkawy, 2020). Spatial-spectral images were generated to highlight the variations in the reflectance qualities of malignant versus normal tissue. It has been found that the ideal bandwidth was proposed to be the overlaid spectral range 420–620 nm. The tumor location of the ex-vivo breast sample was successfully classified by the HS imaging system, with sensitivity and specificity of 95 percent and 96 percent, respectively. The combination of deep learning (2D-CNN) and HSI was used to differentiate the tumor, and normal cells and AUC of 0.89 were obtained (Ortega et al., 2020).

Non-melanoma skin cancer (NMSC), the fifth most prevalent type of cancer worldwide, and melanoma, skin cancer (melanoma), 21st most common worldwide, are the two types of skin cancer (Bray et al., 2018). A dermatological acquisition system based on HSI was created by combining unsupervised and supervised algorithms. 125 spectral bands ranging from 450 and 950 nm were captured for their study. A total number of 76 HS Pigmented skin lesions images were used from different 61 patients, and these images were labeled and classed as benign or malignant. The sensitivity and specificity ratings for distinguishing cancer and benign cells were 87.5% and 100%, respectively (Leon et al., 2020). HSI has also been shown to be capable of detecting skin cancer in real time. Torti et al. for example, created a parallel classification pipeline based on K-means and support vector machine (SVM) for skin cancer detection using HSI that can categorize an image in less than 1 second (Torti et al., 2020). Fig. 6 depicts a block diagram of the HS dermatological classification framework.

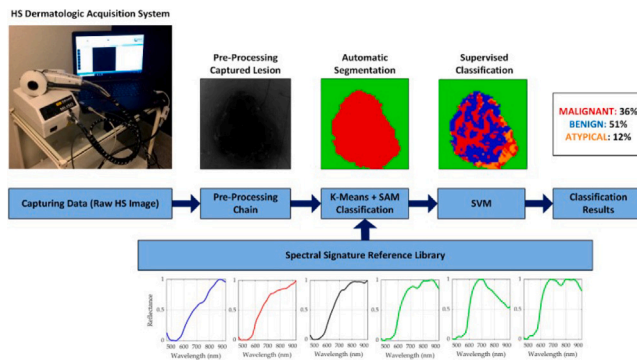


**Fig. 6.** Block diagram of the HS dermatologic classification framework (Torti et al., 2020).

Colon cancer metastasis in the liver was also diagnosed using HSI by Kopriva et al. (2019). In their study, the maximum angle between cancer and non-cancer spectra is 1.02 degrees less than the smallest angle between cancer and non-cancer spectra. As a result, the spectrum angle mapper was employed for pixel-based cancer diagnosis, with sensitivity ranging from 81.23 percent to 97.12 percent, specificity from 85.85 percent to 97.3 percent, and accuracy from 86.85 percent to 96.92 percent.

#### Retinal diseases

Direct retina imaging is used routinely to diagnose and test for retinal illness utilizing tools such as color fundus cameras and scanning laser ophthalmoscopes. Spectrum imaging of the retina involves the acquisition of spectral images with increased spectral detail, which bears the prospect of enhanced classification of retinal biochemistry. Khoobehi, Beach, and Kawano (2004) investigated a hyperspectral imaging approach where a fundus camera was used for measuring relative spatial changes in retinal oxygen saturation. According to their findings, hyperspectral imaging can be used to assess and map relative oxygen saturation in retinal structures and the optic nerve head (ONH) in nonhuman primate eyes. The oxygen saturation measurement result was found to overlap satisfactorily with the in vitro analysis, although more attention should be paid to retinal blood vessels. Lim et al. studied retinal hyperspectral imaging in the 6 to 17 months old 5\*FAD mouse model of Alzheimer's disease (AD) (Lim et al., 2021).

#### Diabetic foot

Diabetic foot ulceration is a significant diabetes complication, with diabetics having a 25% lifetime risk of developing a foot ulcer that needs amputation of the affected limb (Singh, Armstrong, & Lipsky, 2005). Khaodhia et al. conducted one of the first clinical studies in 2007 on the efficacy of hyperspectral technology (HT) to assess tissue oxy- and deoxyhemoglobin to predict diabetic foot ulcer healing and obtained the HT index's sensitivity, specificity, and positive and negative predictive values for predicting healing were 93%, 86%, 93%, and 86%, respectively (Khaodhia et al., 2007). For the first time, it has been demonstrated that foot ulceration can be managed with the use of HT, and HT can detect microvascular anomalies and tissue oxygenation in the diabetic foot and predict ulcer healing. Nouvong et al. did a similar trial in 2009, in which 66 patients with type 1 and type 2 diabetes were enrolled and tracked during a 24-week period, achieving sensitivity and specificity of 80% and 74%, respectively, based on the healing index (Nouvong et al., 2009).

#### Surgical guidance

As an intraoperative guidance tool in several surgical disciplines, imaging spectroscopy technology is becoming increasingly popular among research teams. Imaging spectroscopy technology has been successfully used in various surgical fields, including reconstructive surgery (Nouri, Lucas, & Treuillet, 2016), urology (Akbari et al., 2012),

and neurosurgery (Barberio et al., 2020). The trending surgical guidance applications will be explained in the following sections, namely, mastectomy, gall bladder surgery, and renal surgery.

#### Mastectomy

Patients with early-stage breast cancer could select between a lumpectomy with radiation or a mastectomy alone. Even though both operations had the same survival rates, re-excision rates in breast lumpectomy were stated to be approximately 40% in Fisher et al. (2002). Residual tumors, which were not visible to the surgeon during the procedure, were usually identified near the resected material's periphery. As a result, intraoperative tumor assessment is vital for full resection. Kho et al. recently investigated the application of imaging spectroscopy for human breast margin assessment using specimens from 18 patients with a dataset of 22,000 spectra connected with histology using support vector machine (Kho et al., 2019). Their study was tested on six lumpectomy specimens. With accuracies of 93%, 84%, 70%, and 99%, invasive carcinoma, ductal carcinoma in situ, connective tissue, and adipose tissue were correctly classified as a tumor or healthy tissue, respectively, demonstrating the potential use of imaging spectroscopy for margin assessment during breast-conserving surgery.

#### Gall bladder

Gallbladder diseases frequently demand surgical removal of the gallbladder, which is the most performed procedure in the United States and involves abdominal incisions ranging from 5 to 10 mm during the process. Since the surgical equipment and video camera are placed where the surgery happens, the surgeon is no longer capable of having tactile feedback during the operation. The traditional video camera used through an endoscope to locate the biliary tree had low picture contrast. In animals, the viability of employing HSI for intraoperative tumor margin delineation demonstrated promising results to overcome the issue mentioned earlier during the surgery (Lu, Halig, Wang, Chen, & Fei, 2014). In Zuzak et al. (2007), an endoscope-based HSI system was created to identify tissue anatomy and molecular content during a laparoscopic operation on swine utilizing near-IR laparoscopic HSI without using a radioactive contrast agent. It was discovered that lipids that absorb light at 930 nm could be utilized as an inherent biomarker for imaging the lipid-containing bile ducts that connect the gall bladder, and the surgeon must know the position before cutting during cholecystectomy.

#### Renal surgery

HSI was also used to make real-time surgical procedures use practical for renal surgery. For instance, Campbell et al. (2009) advocated using Laparoscopic Partial Nephrectomy (LPN) to diagnose renal cortical cancers. Olweny et al. (2013) used Digital Light Processing (DLP) based HSI for computer-aided LPN to characterize renal oxygenation. The clinical trial included eighteen individuals. The suggested approach was capable of characterizing dynamic changes in renal oxygenation during LPN. The surgeon can benefit from intraoperative tissue and perfusion evaluations in a variety of ways.

#### 4.2. Airborne systems

In airborne systems, hyperspectral imaging has numerous applications. Environmental monitoring, mineral exploration, agriculture, defense and security, and archaeology are all possible applications. Hyperspectral imaging, for example, can detect pollutants in the environment, identify mineral deposits, monitor crop health, track enemy activity, and map archaeological sites.

##### 4.2.1. Agriculture

The worldwide agricultural sector is facing a variety of challenges, including a fast-expanding population and natural resource depletion. These are critical issues that must be addressed as the global demand for crop production is expected to double by 2050 according to a study in Tilman, Balzer, Hill, and Befort (2011). Improved farming techniques

utilizing hyperspectral image analysis are a promising attempt to address these difficulties due to imaging spectroscopy's ability to capture fine-scale spectral properties of targets. As a result, it can accurately and timely detect the crop's physiological status, anomalies (Catalano et al., 2022), and generate early alarms, if needed. An interesting study was done by Arink, Khan, and Polder (2021) to understand how much of the interior of the tomato contributes to the measured spectra and helps in determining its sweetness. Such an understanding is important when considering the applications of imaging spectroscopy for the determination of various traits in the quality estimation of post-harvest food products. Another quality factor in the food processing pipeline is to determine the foreign materials in the product. As an example, Saeidan, Khojastehpour, Golzarian, Mooenfarad, and Khan (2021) used imaging spectroscopy to determine the presence of foreign materials in cocoa beans. Such foreign materials have the same shape and size as cocoa beans and are therefore very difficult to detect through color imaging.

Crop monitoring based on the crop's biochemical and biophysical properties is one of the significant applications of imaging spectroscopy in agriculture (Mishra, Lohumi, Ahmad Khan, & Nordon, 2020). The chlorophyll content of leaves is an important biochemical property that influences vegetation photosynthetic capacity and crop efficiency (Jarmer, 2013). As a necessary consequence, estimating the content of biochemical properties, such as chlorophyll and nitrogen content in a winter wheat field (Oppelt & Mauser, 2004) and a rice field using Hyperion data (Moharana & Dutta, 2016) is critical.

The one-sided area of leaves per unit of ground area is commonly denoted as the leaf area index (LAI). The LAI is a fundamental vegetation biophysical parameter that is strongly related to crop biomass and yield (Chiozza, Parmley, Higgins, Singh, & Miguez, 2021). As a result, hyperspectral remote sensing has been intensively researched in order to determine the LAI of various crops as it relates to vegetative productivity. Yu et al. for example, develop a theoretical foundation for using unmanned aerial vehicle (UAV) hyperspectral remote sensing to invert rice biochemical parameters in a non-destructive and fast manner to analyze LAI, leaf chlorophyll content, canopy water content, and dry matter content in order to better understand rice growth (Fenghua et al., 2017). LAI estimation for winter wheat Siegmann, Jarmer, Beyer, and Ehlers (2015) using EmMap images and barley (Jarmer, 2013) for monitoring the spatial patterns of crop variables were also studied using hyperspectral images in precision agriculture. Additionally, Locherer et al. used EnMAP data to estimate LAI in mixed agricultural fields and compared the accuracy of the results to that of LAI estimation using airborne data for mixed agricultural fields (Locherer, Hank, Danner, & Mauser, 2015).

As another application of imaging spectroscopy in agriculture, precision farming comprises evaluating crop nutrient levels and making specific resource management suggestions based on crop requirements, with the goal of reducing environmental impact (Cilia et al., 2014). Imaging spectroscopy is commonly used by researchers to forecast nitrogen content in a variety of crops. Plant nitrogen level is assessed in a maize field using hyperspectral images captured 300 m above the experimental site and used to measure greenness, chlorophyll, and photochemical indices, as well as develop nitrogen fertilizer recommendations (Quemada, Gabriel, & Zarco-Tejada, 2014). The acquisition of remotely sensed data from more than one time period is known as multitemporal imaging. Castaldi et al. used multi-temporal satellite-based multispectral and hyperspectral images to estimate nitrogen content at various growth stages throughout two wheat growing seasons in Italy and discovered that band selection influenced estimation accuracy at different phenological phases (Castaldi, Castrignanò, & Casa, 2016). This is because the high dimensionality and high correlation of hyperspectral images are the main issues affecting estimation accuracy, and one way to address these issues is to perform band selection (BS), which involves removing a portion of the spectral bands from hyperspectral images while retaining both useful and original information.

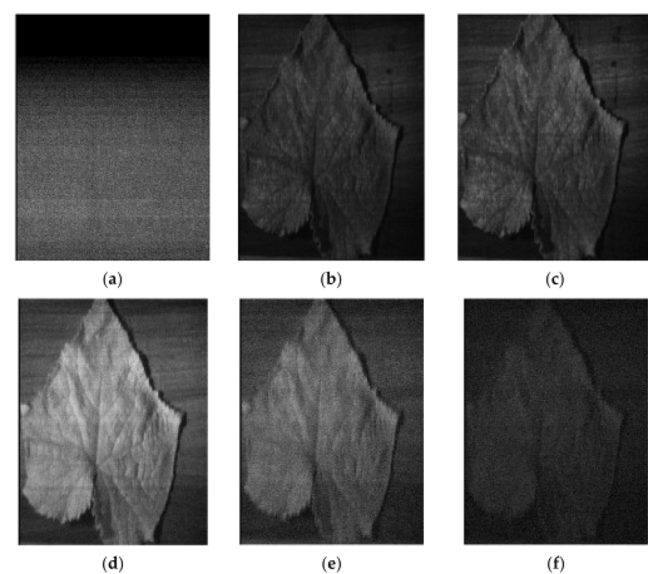


**Fig. 7.** Some examples of the hyperspectral images of cucumber leaves in the range of wavelengths from 400 to 1100 nm: (a) 420 nm; (b) 540 nm; (c) 690 nm; (d) 800 nm; (e) 950 nm; (f) 1040 nm (Sabzi et al., 2021).

Early excess nitrogen in cucumber plants was detected at a rate of 96.11 percent classification accuracy utilizing artificial neural networks and the imperialist competitive algorithm (ANN-ICA) (Sabzi et al., 2021). The images in their investigation were taken with a hyperspectral camera (in the range of 400–1100 nm), as illustrated in Fig. 4. The most efficient wavelengths for early detection of excess nitrogen were determined to be 715, 783, and 821 nm (see Figs. 7 and 8).

Rice nitrogen status is also estimated and monitored by researchers using UAV-based hyperspectral images (Zheng et al., 2016) and airborne hyperspectral images along with multivariable analysis (Ryu, Suguri, & Umeda, 2011). As a result, when a considerable amount of spectrum information is employed in imaging spectroscopy, crop nutrient levels can be accurately assessed, and fertilizer treatment strategies can be advised while also taking into account soil moisture and topographic circumstances.

Another important application is crop disease detection because it has a direct negative impact on yield. Disease detection using hyperspectral images is in high demand for a variety of crops. Because hyperspectral signals are sensitive to small changes caused by disease or stress, they can be used to estimate crop growth status variation while accounting for nutrient deficiency (Thomas et al., 2018). Fusarium head blight classification index in winter wheat using close-range hyperspectral imaging detected in Zhang et al. (2019), airborne hyperspectral images to detect the signal of Ostrinia nubilalis in a cornfield is utilized in Carroll et al. (2008), Nagasubramanian et al. detected charcoal rot in soybeans using close-range hyperspectral imaging (Nagasubramanian et al., 2019), sugarcane areas affected by orange rust diseases using EO-1 Hyperion data in Mackay, Queensland is detected in Apan, Held, Phinn, and Markley (2004).

Imaging spectroscopy can also aid in the investigation of soil properties. Casa, Castaldi, Pascucci, Basso, and Pignatti (2013) collected soil samples in central Italy and then investigated available soil water content, clay content, and sand content using a fusion of CHRIS-PROBA images for satellite image acquisition and soil geophysical data obtained using the automatic resistivity profiling method (ARP). Soil Organic Carbon (SOC) is an important component of soil fertility, and crop yield is highly dependent on SOC. If the images are taken during the crop's non-growing season, hyperspectral imaging may be a viable option for measuring SOC. Zhang, Li, and Zheng (2013) for example, used EO-1 Hyperion images obtained in Central Indiana to

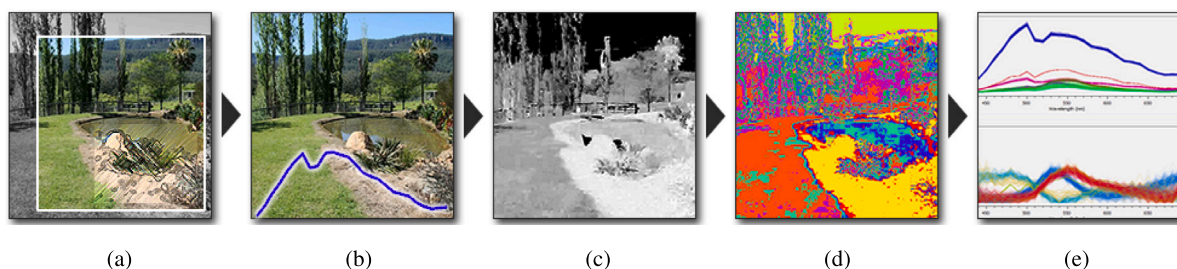


**Fig. 8.** Shows the processing pipeline of a hyperspectral image using AI tools: (a) represents the pre-processing, (b) represents the illumination recovery, (c) represents the reflectance recovery, (d) represents the area clustering, and (e) analysis the different statistical values of the hyperspectral image in the form of a graph (Habili & Oorloff, 2015).

estimate soil moisture, organic matter, total carbon, total phosphorus, total nitrogen, and clay content. This estimation was based on partial least squares (PLS) regression, and it was demonstrated that spectral resolution influences PLS performance.

Hbirkou et al. used images from the aircraft-mounted hyperspectral sensor HyMap (450–2500 nm) to predict SOC in agricultural fields (Hbirkou, Pätzold, Mahlein, & Welp, 2012). Airborne hyperspectral imagery in conjunction with topographic information extracted from LIDAR images to map soil organic matter and automated machine learning approaches to examine the link between soil spectral reflectance and soil organic matter is used in Gedminas and Martin (2019). Topsoil organic carbon was estimated using hyperspectral data collected by an Airborne Hyperspectral Scanner (AHS) and the Hyperion satellite hyperspectral sensor (Hyperion), both of which have different spectral and spatial resolutions (Peón et al., 2017). These studies demonstrate that imaging spectroscopy is a useful tool that can be used to investigate various soil properties.

#### 4.2.2. Environment monitoring

For informed and effective spatial-temporal ecosystem monitoring, while satellite-based earth observation data provide cost-efficient and timely information, it is usually limited because of spatial and spectral information range. Since the last decade, HSI has emerged as a promising source for monitoring a wide range of ecosystems (i.e., terrestrial, forest, grassland, desert, tundra, freshwater, and marine ecosystems) (Abbas et al., 2021; Dumke et al., 2018; Freitas et al., 2021; Rast & Painter, 2019). In this regard, for example, Abbas et al. (2021), performed a study in which they prepared a hyperspectral library for 19 different species of urban trees in the Hong Kong region. In their study, they adopted the Deep Neural Network classification model and obtained accuracy between 85% to 96% for different seasons. Through their study, they improved the understanding of the seasonal response of different urban tree species in Hong Kong and prepared up-to-date hyperspectral urban tree archives for monitoring purposes.

Furthermore, HSI also provides valuable results for conservation-based mangrove studies, which are one of the most important wetlands in global coastal regions. Cao et al. (2018) used HSI sensor (UHD 185) mounted on a UAV to perform object-based mangroves mapping. To achieve the outcome, they utilized a classification and regression tree (CART), and correlation-based feature selection (CFS) algorithm for optimal feature selection for mangrove classification purposes and obtained Kappa ( $\kappa$ ) = 0.79 and  $k$  = 0.87 (representing 80%–90% accuracy) for the k-nearest neighbor (KNN) and support vector machine (SVM) classifiers, respectively. In another study, Osei Darko, Kalacska, Arroyo-Mora, and Fagan (2021), achieved mangroves classification using airborne HSI and statistical physics models (Mean Information Gain—MIG) and Marginal Entropy (ME). As a result, they achieved the highest overall accuracy of 98.8% using the visible-near infrared (VNIR) reflectance along with MIG and ME.

#### 4.2.3. Climate change

Airborne Hyperspectral Scanner (AHS) thermal-infrared (TIR) provides promising results for the characterization of industrial-based

pollutants in the atmosphere responsible for urban microclimate defacement (Tratt, Buckland, Hall, Keim, & Johnson, 2016), which is further associated with numerous health-related issues. Gaseous pollutants, such as greenhouse gases (GHGs), including major proportions of methane ( $\text{CH}_4$ ) and carbon dioxide ( $\text{CO}_2$ ) are primarily responsible for climate change causing a rise in global temperature. Relatedly, Urban Green Space (UGS) is an important component of cities that helps to reduce urban heating, enhance carbon sequestration, air and water pollution remediation, flood abatement, noise reduction, human mental health, wildlife habitat and pollution reduction (Kothencz, Kolcsár, Cabrera-Barona, & Szilassi, 2017). But with the recent upsurge in urbanization rate all around the world, UGS is decreasing. For urban microclimate stability, UGS is an important parameter, and previously many airborne datasets have been used for UGS monitoring but nearly all fail to some extent when differentiating various UGS classes (i.e., trees from grassland, etc.) (Chen et al., 2018). HSI sensors provide the detailed spectral and spatial context of UGS and allow monitoring of UGS types as well. For example, Lv et al. (2009) performed UGS mapping using the Multiple Endmember Spectral Mixture Analysis (MESMA) and Hyperion HSI over the Palo Alto region in the United States. They achieved an overall accuracy of 85% and concluded that MESMA is the best-suited technique for differentiating UGS from heterogeneous urban landscapes.

Additionally, in the context of the urban climate, Urban Heat Island (UHI) is a well-known phenomenon in which the temperature of metropolitan areas is considerably higher than the surrounding rural areas. The Airborne Hyperspectral Scanner Thermal Infrared (AHS-TIR) is well known for its capability to quantify bio-geophysical variables such as Land Surface Temperature (LST). In the past, HSI has been used to study UHI. For example Mongeau et al. (2017) utilized airborne HSI data to prepare a 3D intra-urban heat island patterns map and identified air microparticles responsible for temperature upsurge in the Ville de Montreal region. In another study, Ghandehari et al. (2016) utilized HSI to study urban gaseous emissions using 128 HSI spectral bands (between 7.4 to 13.2 micrometers). Through their study, they analyzed the emission, transportation, and dispersal of 10 different gases. Besides this, they further performed thermal analysis (emissivity, surface temperatures, Heating, Ventilating, and Air Conditioning—HVAC—operations) on 400 buildings in New York City.

While airborne data allows classification of environmental systems (e.g., mangroves sites) with good accuracy, HSI provides valuable results when it comes to pest and disease detection in such systems—giving HSI an upper hand as compared with other earth observation products. Jiang et al. (2021), for example, analyzed spatial and spectral characteristics of diseased mangroves using the successive projection algorithm (SPA) along with the Random Forest (RF). Their findings revealed that there exists an inverse relationship between mangrove leaf traits and pests and disease severity and the SPA-RF model. They further concluded that airborne hyperspectral data had great potential in preparing an early warning system for mangrove pest and disease detection at the regional level, providing progressive opportunities for the application of HSI in environmental monitoring and management.

**Table 3**  
Existing HSI databases.

Reference	Featured Scenes	Number of Images	Spectral range	Spectral Channels	Spatial Resolution	Applications
AeroRIT (Rangnekar, Mokashi, Ientilucci, Kanan, & Hoffman, 2020)	Environment remote sensing	-	397–1003 nm	372	0.4 m	Segmentation and Classification
ARAD-HS (Arad et al., 2022)	Natural images	1000	400–700 nm	16	512 × 482	Classification and Detection
AVIRIS (Green & Boardman, 2000)	Agriculture and land cover	10300	400–2500 nm	224	20 m for Indian Pines	Anomaly Detection and Classification
Botswana (Hyperspectral Remote Sensing Scenes, 2020)	Earth Observation and Climate Change	3248	400–2500 nm	242	1496 × 256	Classification
BGU-HS (Yasuma, Mitsunaga, Iso, & Nayar, 2010)	Environment	286	400–700	31	1392 × 1300	Image reconstruction and super-resolution
Chikusei (Yokoya & Iwasaki, 2016)	Agriculture	77592	363–1018	128	2517 × 2335	Classification and image super-resolution
Database of Nordic sawn timbers (Hirvonen et al., 2014)	Wood analysis	107	300–2500 nm	-	-	Analysis and detection
Historical documents (Kim, Zhuo, Deng, Fu, & Brown, 2010)	Historical document Analysis	-	365–1100 nm	70+	256 × 256	Classification, detection, and segmentation
HyTexLi (Khan, Mioubi, Mathon, Thomas, & Hardeberg, 2018)	Texture Analysis and Material Identification	112	405–995 nm	186	1800 × 2000	Classification and identification
Hyperspectral Human Brain Image Database (Fabelo et al., 2019)	Brain cancer detection	36	400–1000 nm	-	2–3 nm	Classification and detection
Hyperspectral Dermoscopy Dataset (Gu, Partridge, & Zhou, 2018)	Melanoma detection	330	465–630 nm	16	512 × 272 pixels	Classification and detection
ICVL (Arad & Ben-Shahar, 2016)	Environment	203	1000–1300 nm	31	1392 × 1300	Classification
IVision HHID (Islam et al., 2022)	Document forensic analysis	270	478–901 nm	149	512 × 650 pixel	Classification and recognition
ISET (Xiao, Farrell, Catrysse, & Wandell, 2009)	Face, Environment, and Food	-	400–700 nm	-	-	Classification and segmentation
KAUST-HS (Li et al., 2021)	Multiple (Vehicle, Environment, Food)	409	400–730	34	512 × 512	Classification and detection
ROSIS-3 (Ghamisi et al., 2017)	Urban data classification	103551	400–2500 nm	210	1.3 m	Classification
SALINAS (Zheng, Zhong, Ma, & Zhang, 2020)	Agriculture	217	380–2500 nm	224	3.7 m	Classification and analysis
Spectral (Hirvonen et al., 2014)	Wood	107	300–2500 nm	-	-	Analysis and classification
SpecTex (Mirhashemi, 2018)	Spectral texture analysis	60	400–780 nm	76	640 × 640	Analysis and classification
University of Pavia (UP) (Chakraborty & Trehan, 2021)	Agriculture	43000	430–860 nm	103	610 × 340	Classification
WHU (Zhong et al., 2018)	Agriculture	204542	400–1000 nm	270	550 × 400	Classification and segmentation
Z.pan (Di, Zhang, Zhang, & Pan, 2010)	Face recognition	300	700–1000 nm	33	-	Classification and recognition

#### 4.2.4. Minerals

Remote sensing of minerals works on the basic principle in which different minerals have specific spectral characteristic, which can be detected through remote sensing sensor. While multispectral-based airborne sensors fail to explore this area of research due to limit spectral differentiating ability, HSI has been proved to be among the best cost-efficient options to explore mineral ores (Peyghambari & Zhang, 2021). HSI data between 0.4 to 2.5 μm visible and near-infrared (VNIR) and short-wave infrared (SWIR) is best suited for mineral exploration. For example, Bishop, Liu, and Mason (2011) performed a localized study in Pulang region in China. They used Hyperion HSI data, along with the Advanced Spaceborne Thermal Emission and Reflection Radiometer (ASTER) data. They first used ASTER images to identify mineral target areas and then used Spectral Angle Mapper (SAM) and Mixture Tuned Matched Filtering (MTMF) techniques to discriminate and map mineral species with high spatial details.

Similarly, Wan, Fan, and Jin (2021), performed over Huaniushan, Gansu Province of China presented a methodology for mapping minerals (gold, silver, lead, and zinc) ores using airborne HSI data. The findings of their study revealed that spectral angle mapping, minimum noise fraction transform, and mixed-tuned matched filtering were the most suitable classification techniques for extracting mineral deposit information with an accuracy of 80% using HIS data.

## 5. Hyperspectral databases and AI tools

In this section, we discuss open-source hyperspectral databases and AI tools to process hyperspectral images.

### 5.1. Hyperspectral datasets

Many hyperspectral databases have been developed in the last two decades and most of them are publicly available, as shown in Table 3. Some of them are discussed below:

#### 5.1.1. AeroRIT dataset

The AeroRIT hyperspectral dataset (Rangnekar et al., 2020) is designed to facilitate aerial hyperspectral scene understanding. The dataset includes a radiance-calibrated hyperspectral scene sampled at every 10th band, between 397–1003 nm. The semantic map pixels were labeled with ENVI 4.8.2, using individual hyperspectral signatures and the geo-registered RGB images as references. This dataset is a significant step towards developing robust algorithms for hyperspectral airborne sensing that can perform advanced tasks like vehicle tracking and occlusion handling.

#### 5.1.2. ARAD-HS dataset

The ARAD-HS dataset (Arad et al., 2022), also known as the ARAD 1 K natural spectral image dataset, is the largest collection of natural hyperspectral images published in June 2022. The dataset contains 950 publicly available train images and 50 test images. The publicly available images have been published as 1-channel hyperspectral images in the 400–700 nm range and 16-channel multi-spectral images in the range of 400–1000 nm.

#### 5.1.3. AVIRIS dataset

The Airborne Visible InfraRed Imaging Spectrometer (AVIRIS) dataset is a collection of hyperspectral images in 224 contiguous

spectral channels with wavelengths from 400 to 2500 nanometers, developed by National Aeronautics and Space Administration (NASA), USA. The main objective of the AVIRIS project is to identify, measure, and monitor constituents of the Earth's surface and atmosphere based on molecular absorption and particle scattering signatures. Research with AVIRIS data is predominantly focused on understanding processes related to the global environment and climate change. The AVIRIS dataset is available for download from the AVIRIS Data Portal and the AVIRIS-NG Data Portal. The data can be used for a wide range of applications, including environmental studies, and climate change research.

#### 5.1.4. Chikusei dataset

The Chikusei Dataset ([Yokoya & Iwasaki, 2016](#)) is an airborne hyperspectral dataset, captured by the Headwall Hyperspec-VNIR-C imaging sensor over agricultural and urban areas in Chikusei, Ibaraki, Japan. Ground truth of 19 classes was collected via a field survey and visual inspection using high-resolution color images. The dataset has been used for various research purposes, including image super-resolution and image classification.

#### 5.1.5. ICVL hyperspectral database

The ICVL database ([Arad & Ben-Shahar, 2016](#)) includes a variety of scene images ([Arad & Ben-Shahar, 2016](#)). A Specim PS Kappa DX4 hyperspectral camera and a rotating stage for spatial scanning were used to capture the images. Images were obtained with a spatial resolution of  $1392 \times 1300$  over 519 spectral bands (400–1000 nm at roughly 1.25 nm increments). The (.raw) files include raw ENVI data from the camera, whereas the (.hdr) files contain the headers needed to decode it. The database contains several datasets, including Botswana ([Hyperspectral Remote Sensing Scenes, 2020](#)), acquired by the NASA EO-1 satellite over the Okavango Delta. Botswana contains 200 images, and it is used for hyperspectral image reconstruction from RGB images.

#### 5.1.6. Spectral laboratory

The Spectral Laboratory at the University of Eastern Finland has collected a variety of spectral datasets [Spectral Color Research Group](#), including a dataset for spectral images related to oral and dental health, spectral images of Nordic sawn timbers ([Garcia Peraza Herrera, Horgan, Ourselin, Ebner, & Vercauteren, 2023](#)), hyperspectral images of textile ([Porebski, Alimoussa, & Vandenbroucke, 2022](#)), and religious icons ([Mirhashemi, 2019](#)). These datasets can be used for research in medical, material science, and texture analysis.

#### 5.1.7. HyTexiLa

The Hyperspectral Texture images acquired in Laboratory (HyTexiLa) dataset provides high spectral and spatial resolution reflectance images of 112 materials to study spatial and spectral textures. The data is in the range from 405.37 nm to 995.83 nm at 3.19 nm intervals and 186 channels. The dataset consists of high-resolution images of food, stone, vegetation, and wood categories.

#### 5.1.8. SpecTex

HyperSpectral Texture Image Database SpecTex is a database of spectral images that includes sixty textile samples with various texture patterns, developed for spectral texture analysis. The image cubes are  $640 \times 640 \times 39$  in dimension, and the spectral data is captured in visible wavelengths ranging from 400 nm to 780 nm at 5 nm intervals ([Hirvonen et al., 2014](#)).

#### 5.1.9. Hyperspectral datasets for forensic analysis

**iVision HHD** ([Islam et al., 2022](#)) is a dataset of handwritten document images, developed by the Institute of Space Technology, Islam-

abad, Pakistan, and Wageningen University & Research, the Netherlands. The dataset contains handwriting samples from 54 subjects. The individuals belong to different age groups, and professions, and have different writing patterns. Each hyperspectral cube in the collection has a spatial resolution of  $512 \times 650$  pixels and 149 spectral channels in the 478–901 nm spectral region. This dataset can be used for forensic examination of document images, including, writer identification, handwritten optical character recognition, and ink mismatch detection. Other hyperspectral document image datasets include ([Kim et al., 2010](#)) for historical document image analysis, and [Borba, Jawhari, Honorato, and de Juan \(2017\)](#) for forensic analysis of documents.

#### 5.1.10. Hyperspectral medical images datasets

Several hyperspectral medical image datasets have been developed to facilitate research in this area:

- **Hyperspectral Brain Dataset:** This public database contains in-vivo hyperspectral human brain images. It was created for research in brain cancer detection, and it contains 36 images in the range of 400–1100 nm, with a spectral resolution of 2–3 nm ([Fabelo et al., 2019](#)).
- **Hyperspectral Dermoscopy Dataset:** This dataset ([Gu et al., 2018](#)) provides hyperspectral images for early screening of skin cancers using image-based approaches. It contains 330 images, in the range of 465–630 nm, containing 16 spectral channels, with a spatial resolution of  $512 \times 512$ .

#### 5.1.11. Hyperspectral datasets for agriculture

There are various hyperspectral imaging datasets for agriculture, some of them are discussed below:

- **University of Pavia:** The Pavian University dataset contains 103 spectral bands, spatial resolution of  $610 \times 340$ , with a geometric resolution of 1.3 m, containing about 43000 samples of nine different classes.
- **Salinas Dataset:** Salinas scene is a hyperspectral dataset collected by the 224-band AVIRIS sensor over Salinas Valley, California, containing 217 samples, with a spectral range of  $380 \times 2500$  nm and 224 spectral channels. It includes vegetables, bare soils, and vineyard fields. Salinas ground-truth contains 16 classes.
- **WHU Dataset:** This dataset ([Zhong et al., 2018](#)) is captured using UAVs and lightweight hyperspectral imaging sensors, within the spectral range of 400–100 nm, 270n spectral bands, and spatial resolution of  $550 \times 400$  nm.

#### 5.1.12. ISET hyperspectral database

This is a set of ISET hyperspectral scenes created from data acquired using a hyperspectral imaging system (Hyspex VNIR-1600) that detects image radiance in narrow bands spanning from 400 to 1000 nm ([Xiao et al., 2009](#)). There are four main types of categories in the ISET hyperspectral database with a different number of scenes.

- **ISET hyperspectral scene data for landscapes:** A collection of hyperspectral image data has been made accessible for use in imaging system simulation. Landscapes and buildings are also included in the collection. The “montage.jpg” file is a collection of monochromatic scenes. A HySpex line-scan imaging spectrometer was used to collect the images, which cover the spectral spans from 400 nm to 950 nm.
- **ISET scenes with fruits and calibration charts:** A bundle of hyperspectral image data is used in the development of imaging systems. The package comes with fruit images and performance charts. The images were captured using a HySpex line-scan imaging spectrometer with spectral ranges of 400 nm to 950 nm. Multicolor images of the scene’s contents may be found in the “montage.jpg” file.

**Table 4**  
Existing AI-based software protocols for HSI.

Reference	Description	Github link
AVHYAS (Lyngdoh et al., 2021)	An Open Source QGIS tool for Advanced Hyperspectral Image Analysis	AVHYAS
DeepHyperX (Audebert, Le Saux, & Lefèvre, 2019)	A PyTorch based software toolbox for hyperspectral data classification	DeepHyperX
DIP-HyperKite (Bandara, Valanarasu, & Patel, 2021)	Hyperspectral PanSharpening Based on Improved Deep Image Prior and Residual Reconstruction	DIP-HyperKite
3D-HyperGAMO (Roy, Haut, Paoletti, Dubey, & Plaza, 2022)	Generative Adversarial Network for minority class oversampling in Hyperspectral image classification	3D-HyperGAMO
Hyperspectral imaging library (Audebert et al., 2019)	A MATLAB toolbox for processing hyperspectral data	–
hsdar (Lehnert et al., 2018)	An R package for processing, feature extraction and classification of hyperspectral data	hsdar
HSImage (Brown & Moser, 2018)	A Python and C++ library for interactive ENVI-BIL hyperspectral images	HSImage
HybridSN (Roy, Krishna, Dubey, & Chaudhuri, 2019)	A spatio-spectral method for HSI classification using Pytorch	HybridSN
Hyperspectral (Vali, Comai, & Matteucci, 2020)	Deep Learning for Land-cover Classification in Hyperspectral Images	Hyperspectral
HSIToolbox (Dhaene, Žižakić, Huang, Li, & Pižurica, 2023)	A web-based application for the classification of hyperspectral images	HSIToolbox
HSI-Tradition-to-Deep (Ahmad et al., 2021)	A Github repo of traditional to Deep learning models for HSI classification	HSI-Traditional-to-Deep
Scyllarus (Habili & Oorloff, 2015)	A C++ API for processing of hyperspectral images	SCYLLARUS
spectrai (Horgan & Bergholt, 2021)	A PyTorch based framework for processing spectral data	spectrai
Specim (Behmann et al., 2018)	A commercial software for hyperspectral imaging	Specim

- ISET scenes of faces at 3M distance:** This data includes 46 pictures of human faces taken at a distance of 3 m. The hyperspectral pictures are organized into six zip files that could be downloaded. A monochromatic picture of the faces is shown in the file “montage.jpg”. A HySpex line-scan imaging spectrometer was used to capture the images, which covered the spectral spans 400 nm to 950 nm.
- ISET hyperspectral scenes of human faces at high resolution, 1M distance:** There are 25 images of human faces in this collection, each collected at a distance of one meter. The hyperspectral images are available for download in six zip files. In the file “montage.jpg”, faces were presented in monochrome. The images were captured using a HySpex line-scan imaging spectrometer, which spanned the spectral spans of 400 nm to 950 nm.

There are hyperspectral datasets for other applications as well, such as face recognition (Di et al., 2010), wood analysis (Hirvonen et al., 2014), and Rosis-3 (Ghamisi et al., 2017) for urban data classification. However, to fully exploit the potential of imaging spectroscopy in various applications, large open-source hyperspectral databases are still needed.

## 5.2. AI software tools for HSI datasets

In the last two decades, several artificial intelligence (AI) based tools are developed to process hyperspectral images as discussed in Table 4. Scyllarus is a set of software tools for processing hyperspectral data and producing useful results (Habili & Oorloff, 2015). Scyllarus offers customers usable data for a variety of applications by utilizing sophisticated and advanced image processing algorithms developed at Data61. Whatever sector you operate in, there is a good chance that imaging spectroscopy can help you. Scyllarus added three frequently used AI tools to the hyperspectral image processing procedure.

### 5.2.1. AVHYAS toolbox

The AVHYAS toolbox is a free and open-source Python-based QGIS plugin for advanced hyperspectral image analysis. It provides a wide range of functions for atmospheric correction, preprocessing, unmixing, classification and regression, deep learning, fusion, spectral indices, and geo-physical applications.

### 5.2.2. Scyllarus C++ API

The Scyllarus (Habili & Oorloff, 2015) C++ API is designed for developers that intend to include hyperspectral processing into their applications. The Scyllarus C++ API contains numerous image-processing capabilities and tools that are used in imaging spectroscopy applications. It imports and saves Hyperspectral Image data in the following formats (HDR (ENVI) flat/raw file, BIL, BSQ, and BIP formats,

and HSZ (Hyperspectral Zip). It has reflectance recovery and automatic illuminant. This tool does not need to be calibrated. It has a rapid estimate approach that uses automatic spectra-based material clustering/segmentation.

### 5.2.3. Scyven (scyllarus visualization environment)

Scyllarus is the founder of this hyperspectral visualization tool. Scyven (Scyllarus Visualization Environment) helps us to examine Hyperspectral images and analyze them to find spectral structures. Scyven is a simple graphical user interface with the tremendous capability of the Scyllarus C++ API. Scyven can be used to find facts about sceneries that the naked eye or typical RGB images could not have. It can increase the use of Hyperspectral image data by using powerful processing techniques. Scyven is compatible with both Windows and Linux, and it does not require any particular hardware to handle data. You can collect data in other places and then import it into Scyven. Automatic Illuminant Recovery, Reflectance Recovery, and Material Discovery are among the features. It uses SAM (Spectral Angle Mapping), SVM (Support Vector Machines), LSU (Linear Spectral Unmixing), and PCA (Principal Component Analysis) techniques for Spectral Library Classification.

The Scyllarus MATLAB Toolbox was created to help researchers with hyperspectral and multispectral image processing techniques. Scyllarus is implemented inside this Toolbox separately from the C++ API. It is more comprehensive and includes features that are not accessible in the C++ API, such as, Deterministic annealing, K-means, Image reformatting, and quantization techniques. It represents spectral data with smooth functions based on Gaussian functions, such as NURBS (Non-uniform Rational B-Splines).

### 5.2.4. Hyperspectral imaging library

The MATLAB toolbox contains various algorithms for hyperspectral data processing and analysis, such as end-member extraction, abundance map estimation, spectral matching, and anomaly detection. The toolbox supports reading and writing hyperspectral data in different file formats, such as NITF, ENVI, TIFF, and MTL.

### 5.2.5. The hsdar package

Hyperspectral data analysis package (Lehnert et al., 2018) in R provides functions for processing, analyzing, and visualizing hyperspectral data in R. The package allows users to perform common tasks such as spectral unmixing, dimensionality reduction, classification and clustering. The package also includes several datasets and examples to demonstrate its functionality and applications.

## 5.3. Deep learning libraries for processing spectral data

There are various deep learning libraries for hyperspectral image analysis. Some of them are given below.

### 5.3.1. Spectrai

It is an open-source deep learning framework designed to train neural networks on spectral data and compare alternative methods. Spectrai includes a variety of spectrum data pre-processing and augmentation methods, as well as neural networks for spectral data, such as spectral (image) denoising, spectral (image) classification, spectral image segmentation, and spectral image super-resolution. Spectrai features both command line and graphical user interfaces (GUI) to let users make models and tune hyperparameters for a variety of applications.

### 5.3.2. DeepHyperX

It is a pytorch-based framework for processing hyperspectral data (Audebert et al., 2019). The tool includes several variants of SVM from scikit-learn and multiple variants of Convolutional neural networks. The program provides various critical hyperspectral analysis tools, such as continuum removal and normalized ratio indices, as well as the integration of two frequently used radiation transfer models.

### 5.3.3. DIP-HyperKite (Bandara et al., 2021)

It is a deep learning-based hyperspectral pan-sharpening method. It is a three-stage method that consists of: Up-sampling the low-resolution hyperspectral image (LR-HSI) to the spatial resolution of the panchromatic image (PAN). Predicting the residual image between the LR-HSI and the up-sampled LR-HSI using a deep convolutional neural network (CNN) and Obtaining the final fused HSI by adding the up-sampled LR-HSI and the predicted residual image.

### 5.3.4. 3D-HyperGAMO (Roy et al., 2022)

The 3D-HyperGAMO toolbox is a software package that uses generative adversarial networks (GANs) to create synthetic samples of minority class data in imbalanced datasets to enhance the performance and robustness of machine learning models. It also offers to algorithms to visualize and explore the generated data in an interactive 3D environment.

Hyperspectral image processing tools help to analyze and manipulate images with hundreds of spectral bands. Some examples of hyperspectral image processing tools are ENVI, MATLAB, Python, and R packages. There are also some commercial software available, specifically designed for hyperspectral data analysis, such as Specim (Behmann et al., 2018).

## 6. Conclusion and future work

In this paper, we presented a thorough review of the contemporary landscape of imaging spectroscopy, placing particular emphasis on hyperspectral and multispectral image acquisition, processing, and analysis. Our comprehensive exploration covered various critical aspects of the field, including applications, pre-processing techniques, the availability of databases, and the ever-evolving landscape of software tools and image processing frameworks for analyzing these images in recent years. We addressed the techniques and challenges involved in the acquisition, processing, and analysis of hyperspectral images across a wide range of application areas, including medicine, food and agriculture, remote sensing of environment, minerals extraction, biometrics, and document analysis. Therefore, our work is expected to provide valuable insights for various interdisciplinary fields.

Despite the growing success of imaging spectroscopy, there are still several core challenges in its hardware acquisition systems, pre-processing and storage techniques. For instance, the high costs of hyperspectral sensors and the absence of common standards for manufacturing these sensors are additional key challenges that limit the widespread adoption of imaging spectroscopy in various areas. While there has been significant advancement in hyperspectral and multispectral sensor technology recently, there is still substantial future research and development potential in this area. Similarly, a large volume of raw data needs to be pre-processed and stored before useful information

can be extracted. Therefore, one potential area requiring special attention is how to reduce the amount of raw imaging spectroscopic data during acquisition and/or storage while retaining high-quality spectral characteristics.

The insufficient availability of publicly accessible labeled imaging spectroscopic data and the difficulty of maintaining such large databases presents another key challenge. Therefore, research in the area of developing large public imaging spectroscopic datasets presents a great opportunity and holds significant value. A related challenge to the limited availability of public databases is the lack of open-source imaging spectroscopy software tools and packages, which hinders the full potential growth of this field. Expanding these resources could lead to more valuable solutions and opportunities for researchers and industry professionals. Therefore, future research in the area of developing large imaging spectroscopic datasets presents a promising opportunity and holds significant value in terms of contribution to the knowledge base.

Developing novel algorithms for near/real-time processing and interpretation of imaging spectroscopy data are other significant challenges, offering tremendous research prospects that can enhance the utilization of this technology for the greater good. For instance, imaging spectroscopy coupled with advanced computer vision algorithms can offer potential solutions for numerous industrial applications, including but not limited to food processing, recycling, mining, and exploration industries. Similarly, when combined with powerful deep learning frameworks capable of processing vast amounts of data for enhanced accuracy, we anticipate that imaging spectroscopy will assume an increasingly dominant and influential role in various airborne and ground-based research and industrial applications. Given the high applicability and significant potential of imaging spectroscopy, further research and development in this field holds the promise of high impact.

## CRediT authorship contribution statement

**Anam Zahra:** Conceptualization, Resources, Writing – original draft. **Rizwan Qureshi:** Conceptualization, Methodology, Writing – original draft, Investigation, Writing – review & editing. **Muhammad Sajjad:** Conceptualization, Resources, Writing – original draft. **Ferhat Sadak:** Conceptualization, Resources, Writing – original draft, Writing – review & editing. **Mehmood Nawaz:** Writing – original draft. **Haris Ahmad Khan:** Conceptualization, Resources, Writing – original draft, Investigation, Writing – review & editing. **Muhammad Uzair:** Conceptualization, Resources, Writing – original draft.

## Declaration of competing interest

The authors declare that they have no known competing financial interests or personal relationships that could have appeared to influence the work reported in this paper.

## Data availability

Data will be made available on request.

## Declaration of Generative AI and AI-assisted technologies in the writing process

The authors have used generative artificial intelligence (AI) and AI-assisted technologies in the writing process and survey preparation. The authors specifically used ChatGPT and Bard to improve readability and language. Authors are ultimately responsible and accountable for the contents of this work.

## References

- Abbas, S., Peng, Q., Wong, M. S., Li, Z., Wang, J., Ng, K. T. K., et al. (2021). Characterizing and classifying urban tree species using bi-monthly terrestrial hyperspectral images in Hong Kong. *ISPRS Journal of Photogrammetry and Remote Sensing*, 177, 204–216.
- Aboughaleb, I. H., Aref, M. H., & El-Sharkawy, Y. H. (2020). Hyperspectral imaging for diagnosis and detection of ex-vivo breast cancer. *Photodiagnosis and Photodynamic Therapy*, 31, Article 101922.
- Acito, N., Diani, M., & Corsini, G. (2011). Signal-dependent noise modeling and model parameter estimation in hyperspectral images. *IEEE Transactions on Geoscience and Remote Sensing*, 49(8), 2957–2971.
- Ahmad, M., Shabbir, S., Roy, S. K., Hong, D., Wu, X., Yao, J., et al. (2021). Hyperspectral image classification—Traditional to deep models: A survey for future prospects. *IEEE Journal of Selected Topics in Applied Earth Observations and Remote Sensing*, 15, 968–999.
- Alkabri, H., Halig, L. V., Schuster, D. M., Osunkoya, A., Master, V., Nieh, P. T., et al. (2012). Hyperspectral imaging and quantitative analysis for prostate cancer detection. *Journal of Biomedical Optics*, 17(7), 076005.
- Alouogianni, E., Ichimura, T., Hamada, M., Ishikawa, M., Murakami, T., Sasaki, A., et al. (2022). Hyperspectral imaging for tumor segmentation on pigmented skin lesions. *Journal of Biomedical Optics*, 27(10), 106007.
- Apan, A., Held, A., Phinn, S., & Markley, J. (2004). Detecting sugarcane 'orange rust' disease using EO-1 Hyperion hyperspectral imagery. *International Journal of Remote Sensing*, 25(2), 489–498.
- Arad, B., & Ben-Shahar, O. (2016). Sparse recovery of hyperspectral signal from natural RGB images. In *European conference on computer vision* (pp. 19–34). Springer.
- Arad, B., Timofte, R., Yahel, R., Morag, N., Bernat, A., Cai, Y., et al. (2022). NTIRE 2022 spectral recovery challenge and data set. In *Proceedings of the IEEE/CVF conference on computer vision and pattern recognition (CVPR) workshops* (pp. 863–881).
- Arellano, P., Tansey, K., Balzter, H., & Boyd, D. S. (2015). Detecting the effects of hydrocarbon pollution in the Amazon forest using hyperspectral satellite images. *Environmental Pollution*, 205, 225–239.
- Arink, M., Khan, H. A., & Polder, G. (2021). Light penetration properties of visible and NIR radiation in tomatoes applied to non-destructive quality assessment. *Engineering Proceedings*, 9(1), <http://dx.doi.org/10.3390/engproc2021009018>, Retrieved from <https://www.mdpi.com/2673-4591/9/1/18>.
- Armin Schneider, H. F. (2017). *Diagnostic procedures* (pp. 87–220). Biomedical Engineering in Gastrointestinal Surgery.
- Audebert, N., Le Saux, B., & Lefèvre, S. (2019). Deep learning for classification of hyperspectral data: A comparative review. *IEEE Geoscience and Remote Sensing Magazine*, 7(2), 159–173.
- Bandara, W. G. C., Valanarasu, J. M. J., & Patel, V. M. (2021). Hyperspectral pansharpening based on improved deep image prior and residual reconstruction. *IEEE Transactions on Geoscience and Remote Sensing*, 60, 1–16.
- Barberio, M., Longo, F., Fiorillo, C., Seeliger, B., Mascagni, P., Agnus, V., et al. (2020). HYPerpectral enhanced reality (HYPER): A physiology-based surgical guidance tool. *Surgical Endoscopy*, 34, 1736–1744.
- Behmann, J., Acebron, K., Emin, D., Bennertz, S., Matsubara, S., Thomas, S., et al. (2018). Specim IQ: evaluation of a new, miniaturized handheld hyperspectral camera and its application for plant phenotyping and disease detection. *Sensors*, 18(2), 441.
- Behmann, J., Mahlein, A.-K., Paulus, S., Kuhlmann, H., Oerke, E.-C., & Plümer, L. (2015). Calibration of hyperspectral close-range pushbroom cameras for plant phenotyping. *ISPRS Journal of Photogrammetry and Remote Sensing*, 106, 172–182.
- Behrend, C. J., Tarnowski, C. P., & Morris, M. D. (2002). Identification of outliers in hyperspectral Raman image data by nearest neighbor comparison. *Applied Spectroscopy*, 56(11), 1458–1461.
- Bendoumi, M. A., He, M., & Mei, S. (2014). Hyperspectral image resolution enhancement using high-resolution multispectral image based on spectral unmixing. *IEEE Transactions on Geoscience and Remote Sensing*, 52(10), 6574–6583.
- Bishop, C. A., Liu, J. G., & Mason, P. J. (2011). Hyperspectral remote sensing for mineral exploration in Pulang, Yunnan Province, China. *International Journal of Remote Sensing*, 32(9), 2409–2426.
- Borba, F. d. S. L., Jawhari, T., Honorato, R. S., & de Juan, A. (2017). Confocal Raman imaging and chemometrics applied to solve forensic document examination involving crossed lines and obliteration cases by a depth profiling study. *Analyst*, 142(7), 1106–1118.
- Bourguignon, S., Mary, D., & Slezak, E. (2010). Sparsity-based denoising of hyperspectral astrophysical data with colored noise: Application to the MUSE instrument. In *2010 2nd workshop on hyperspectral image and signal processing: Evolution in remote sensing* (pp. 1–4). IEEE.
- Bray, F., Ferlay, J., Soerjomataram, I., Siegel, R. L., Torre, L. A., & Jemal, A. (2018). Global cancer statistics 2018: GLOBOCAN estimates of incidence and mortality worldwide for 36 cancers in 185 countries. *CA: A Cancer Journal for Clinicians*, 68(6), 394–424.
- Brown, R. C., & Moser, J. (2018). Hsimage: A Python and C++ library to allow interaction with ENVI-BIL hyperspectral images. *Journal of Open Source Software*, 3(25), 630.
- Campbell, S. C., Novick, A. C., Beldegrun, A., Blute, M. L., Chow, G. K., Derweesh, I. H., et al. (2009). Guideline for management of the clinical T1 renal mass. *The Journal of Urology*, 182(4), 1271–1279.
- Cannistraci, C. V., Monteverchi, F. M., & Alessio, M. (2009). Median-modified Wiener filter provides efficient denoising, preserving spot edge and morphology in 2-DE image processing. *Proteomics*, 9(21), 4908–4919.
- Cao, J., Leng, W., Liu, K., Liu, L., He, Z., & Zhu, Y. (2018). Object-based mangrove species classification using unmanned aerial vehicle hyperspectral images and digital surface models. *Remote Sensing*, 10(1), 89.
- Carroll, M. W., Glaser, J. A., Hellmich, R. L., Hunt, T. E., Sappington, T. W., Calvin, D., et al. (2008). Use of spectral vegetation indices derived from airborne hyperspectral imagery for detection of European corn borer infestation in Iowa corn plots. *Journal of Economic Entomology*, 101(5), 1614–1623.
- Casa, R., Castaldi, F., Pascucci, S., Basso, B., & Pignatti, S. (2013). Geophysical and hyperspectral data fusion techniques for in-field estimation of soil properties. *Vadose Zone Journal*, 12(4), vjz2012–0201.
- Castaldi, F., Castrignanò, A., & Casa, R. (2016). A data fusion and spatial data analysis approach for the estimation of wheat grain nitrogen uptake from satellite data. *International Journal of Remote Sensing*, 37(18), 4317–4336.
- Catalano, C., Paiano, L., Calabrese, F., Cataldo, M., Mancarella, L., & Tommasi, F. (2022). Anomaly detection in smart agriculture systems. *Computers in Industry*, 143, Article 103750.
- Chakraborty, T., & Trehan, U. (2021). SpectralNET: Exploring spatial-spectral WaveletCNN for hyperspectral image classification. *arXiv preprint arXiv:2104.00341*.
- Chen, W., Huang, H., Dong, J., Zhang, Y., Tian, Y., & Yang, Z. (2018). Social functional mapping of urban green space using remote sensing and social sensing data. *ISPRS Journal of Photogrammetry and Remote Sensing*, 146, 436–452.
- Chen, Y.-M., Lai, K.-L., Chen, H.-H., Huang, W.-N., Lin, C.-T., Chao, W.-C., et al. (2020). Hyperspectral imaging for skin assessment in systemic sclerosis: a pilot study. *Rheumatology*, 59(11), 3201–3210.
- Chen, L., Ma, Y., Lian, Y., Zhang, H., Yu, Y., & Lin, Y. (2023). Radiometric normalization using a pseudo- invariant polygon features- based algorithm with contemporaneous sentinel- 2A and landsat- 8 OLI imagery. *Applied Sciences*, 13(4), 2525.
- Cheng, J.-H., Sun, D.-W., Pu, H., & Zhu, Z. (2015). Development of hyperspectral imaging coupled with chemometric analysis to monitor K value for evaluation of chemical spoilage in fish fillets. *Food Chemistry*, 185, 245–253.
- Chiozza, M. V., Parmley, K. A., Higgins, R. H., Singh, A. K., & Miguez, F. E. (2021). Comparative prediction accuracy of hyperspectral bands for different soybean crop variables: From leaf area to seed composition. *Field Crops Research*, 271, Article 108260.
- Cilia, C., Panigada, C., Rossini, M., Meroni, M., Busetto, L., Amaducci, S., et al. (2014). Nitrogen status assessment for variable rate fertilization in maize through hyperspectral imagery. *Remote Sensing*, 6(7), 6549–6565.
- Datta, D., Mallick, P. K., Bhoi, A. K., Ijaz, M. F., Shafi, J., & Choi, J. (2022). Hyperspectral image classification: Potentials, challenges, and future directions. *Computational Intelligence and Neuroscience*, 2022.
- de Oliveira, R. A., Tommaselli, A. M., & Honkavaara, E. (2016). Geometric calibration of a hyperspectral frame camera. *Photogrammetric Record*, 31(155), 325–347.
- Dhaene, Z., Žižák, N., Huang, S., Li, X., & Pižurica, A. (2023). Hstoolbox: A web-based application for the classification of hyperspectral images. *SoftwareX*, 22, Article 101340.
- Dhanoa, M., Lister, S., Sanderson, R., & Barnes, R. (1994). The link between multiplicative scatter correction (MSC) and standard normal variate (SNV) transformations of NIR spectra. *Journal of Near Infrared Spectroscopy*, 2(1), 43–47.
- Di, W., Zhang, L., Zhang, D., & Pan, Q. (2010). Studies on hyperspectral face recognition in visible spectrum with feature band selection. *IEEE Transactions on Systems, Man, and Cybernetics-Part A: Systems and Humans*, 40(6), 1354–1361.
- Dumke, I., Nornes, S. M., Purser, A., Marcon, Y., Ludvigsen, M., Ellefmo, S. L., et al. (2018). First hyperspectral imaging survey of the deep seafloor: High-resolution mapping of manganese nodules. *Remote Sensing of Environment*, 209, 19–30.
- ElMasry, G., Barbin, D. F., Sun, D.-W., & Allen, P. (2012). Meat quality evaluation by hyperspectral imaging technique: an overview. *Critical Reviews in Food Science and Nutrition*, 52(8), 689–711.
- ElMasry, G., & Sun, D.-W. (2010a). Meat quality assessment using a hyperspectral imaging system. In *Hyperspectral imaging for food quality analysis and control* (pp. 175–240). Elsevier.
- ElMasry, G., & Sun, D.-W. (2010b). Principles of hyperspectral imaging technology. In *Hyperspectral imaging for food quality analysis and control* (pp. 3–43). Elsevier.
- Fabelo, H., Ortega, S., Szolna, A., Bulters, D., Piñeiro, J. F., Kabwama, S., et al. (2019). In-vivo hyperspectral human brain image database for brain cancer detection. *IEEE Access*, 7, 39098–39116.
- Fadhlallah Guerri, M., Distante, C., Spagnolo, P., Bougourzi, F., & Taleb-Ahmed, A. (2023). Deep learning techniques for hyperspectral image analysis in agriculture: A review. *arXiv e-prints*, arXiv-2304.
- Farsiu, S., Robinson, M. D., Elad, M., & Milanfar, P. (2004). Fast and robust multiframe super resolution. *IEEE Transactions on Image Processing*, 13(10), 1327–1344.
- Fei, B. (2019). Hyperspectral imaging in medical applications. In *Data handling in science and technology*, vol. 32 (pp. 523–565). Elsevier.

- Feng, Y.-Z., & Sun, D.-W. (2012). Application of hyperspectral imaging in food safety inspection and control: a review. *Critical Reviews in Food Science and Nutrition*, 52(11), 1039–1058.
- Fenghua, Y., Tongyu, X., Wen, D., Hang, M., Guosheng, Z., & Chunling, C. (2017). Radiative transfer models (RTMs) for field phenotyping inversion of rice based on UAV hyperspectral remote sensing. *International Journal of Agricultural and Biological Engineering*, 10(4), 150–157.
- Ferris, D. G., Lawhead, R. A., Dickman, E. D., Holtzapple, N., Miller, J. A., Grogan, S., et al. (2001). Multimodal hyperspectral imaging for the noninvasive diagnosis of cervical neoplasia. *Journal of Lower Genital Tract Disease*, 5(2), 65–72.
- Fisher, B., Anderson, S., Bryant, J., Margolese, R. G., Deutsch, M., Fisher, E. R., et al. (2002). Twenty-year follow-up of a randomized trial comparing total mastectomy, lumpectomy, and lumpectomy plus irradiation for the treatment of invasive breast cancer. *New England Journal of Medicine*, 347(16), 1233–1241.
- Freitas, S., Silva, H., Almeida, C., Viegas, D., Amaral, A., Santos, T., et al. (2021). Hyperspectral imaging system for marine litter detection. In *OCEANS 2021* (pp. 1–6). IEEE.
- Garcia Peraza Herrera, L. C., Horgan, C., Ourselin, S., Ebner, M., & Vercauteren, T. (2023). Hyperspectral image segmentation: a preliminary study on the Oral and Dental Spectral Image Database (ODSI-DB). *Computer Methods in Biomechanics and Biomedical Engineering: Imaging & Visualization*, 11(4), 1290–1298.
- Gedminas, L., & Martin, S. (2019). Soil organic matter mapping using hyperspectral imagery and elevation data. In *2019 IEEE aerospace conference* (pp. 1–8). IEEE.
- Geladi, P., Burger, J., & Lestander, T. (2004). Hyperspectral imaging: calibration problems and solutions. *Chemometrics and Intelligent Laboratory Systems*, 72(2), 209–217.
- Ghamisi, P., Yokoya, N., Li, J., Liao, W., Liu, S., Plaza, J., et al. (2017). Advances in hyperspectral image and signal processing: A comprehensive overview of the state of the art. *IEEE Geoscience and Remote Sensing Magazine*, 5(4), 37–78.
- Ghosh, A., Datta, A., & Ghosh, S. (2013). Self-adaptive differential evolution for feature selection in hyperspectral image data. *Applied Soft Computing*, 13(4), 1969–1977.
- Gonzalez, R. C. (2009). *Digital image processing*. Pearson education india.
- Gonzalez, R. C. (2018). *Digital image processing*. Pearson Education.
- Grabowski, B., Masarczyk, W., Glomb, P., & Mendys, A. (2018). Automatic pigment identification from hyperspectral data. *Journal of Cultural Heritage*, 31, 1–12.
- Green, R. O., & Boardman, J. (2000). Exploration of the relationship between information content and signal-to-noise ratio and spatial resolution in AVIRIS spectral data. *Spectrum*, 7(8).
- Green, R. O., Eastwood, M. L., Sarture, C. M., Chrien, T. G., Aronsson, M., Chippendale, B. J., et al. (1998). Imaging spectroscopy and the airborne visible/infrared imaging spectrometer (AVIRIS). *Remote Sensing of Environment*, 65(3), 227–248.
- Grusche, S. (2014). Basic slit spectroscope reveals three-dimensional scenes through diagonal slices of hyperspectral cubes. *Applied Optics*, 53(20), 4594–4603.
- Gu, Y., Partridge, Y.-P., & Zhou, J. (2018). A hyperspectral dermoscopy dataset for melanoma detection. In *OR 2.0 context-aware operating theaters, computer assisted robotic endoscopy, clinical image-based procedures, and skin image analysis* (pp. 268–276). Springer.
- Guanter, L., Richter, R., & Moreno, J. (2006). Spectral calibration of hyperspectral imagery using atmospheric absorption features. *Applied Optics*, 45(10), 2360–2370.
- Habil, N., & Oorloff, J. (2015). Scyllarus™: From research to commercial software. In *Proceedings of the ASWEC 2015 24th Australasian software engineering conference* (pp. 119–122).
- Hagen, N. A., & Kudenov, M. W. (2013). Review of snapshot spectral imaging technologies. *Optimization and Engineering*, 52(9), Article 090901.
- Hbirkou, C., Pätzold, S., Mahlein, A.-K., & Welp, G. (2012). Airborne hyperspectral imaging of spatial soil organic carbon heterogeneity at the field-scale. *Geoderma*, 175, 21–28.
- He, Z., Liu, H., Wang, Y., & Hu, J. (2017). Generative adversarial networks-based semi-supervised learning for hyperspectral image classification. *Remote Sensing*, 9(10), 1042.
- Heald, M. A., & Marion, J. B. (2012). *Classical electromagnetic radiation*. Courier Corporation.
- Hirvonen, T., Orava, J., Penttinen, N., Luostarinen, K., Hauta-Kasari, M., Sorjonen, M., et al. (2014). Spectral image database for observing the quality of nordic sawn timbers. *Wood Science and Technology*, 48, 995–1003.
- Hong, D., Gao, L., Yao, J., Zhang, B., Plaza, A., & Chanussot, J. (2020). Graph convolutional networks for hyperspectral image classification. *IEEE Transactions on Geoscience and Remote Sensing*, 59(7), 5966–5978.
- Hong, D., Wu, X., Ghamisi, P., Chanussot, J., Yokoya, N., & Zhu, X. X. (2020). Invariant attribute profiles: A spatial-frequency joint feature extractor for hyperspectral image classification. *IEEE Transactions on Geoscience and Remote Sensing*, 58(6), 3791–3808.
- Hong, D., Yokoya, N., Chanussot, J., Xu, J., & Zhu, X. X. (2019). Learning to propagate labels on graphs: An iterative multitask regression framework for semi-supervised hyperspectral dimensionality reduction. *ISPRS Journal of Photogrammetry and Remote Sensing*, 158, 35–49.
- Horgan, C. C., & Bergholt, M. S. (2021). Spectrai: A deep learning framework for spectral data. arXiv preprint arXiv:2108.07595.
- Huang, H., Shi, G., He, H., Duan, Y., & Luo, F. (2019). Dimensionality reduction of hyperspectral imagery based on spatial-spectral manifold learning. *IEEE Transactions on Cybernetics*, 50(6), 2604–2616.
- Hyperspectral Remote Sensing Scenes (2020). Hyperspectral\_Remote\_Sensing\_Scenes. Available online: <http://www.ehu.eus/ccwintco/index.php>. (Accessed 22 April 2020).
- Ilehaq, R., Weinmann, M., Schenk, A., Keller, S., Jutzi, B., & Hinz, S. (2017). Revisiting existing classification approaches for building materials based on hyperspectral data. *The International Archives of the Photogrammetry, Remote Sensing and Spatial Information Sciences*, 42, 65–71.
- Islam, A. U., Khan, M. J., Asad, M., Khan, H. A., & Khurshid, K. (2022). iVision HHID: Handwritten hyperspectral images dataset for benchmarking hyperspectral imaging-based document forensic analysis. *Data in Brief*, 41, Article 107964.
- Jarmer, T. (2013). Spectroscopy and hyperspectral imagery for monitoring summer barley. *International Journal of Remote Sensing*, 34(17), 6067–6078.
- Jia, J., Wang, Y., Chen, J., Guo, R., Shu, R., & Wang, J. (2020). Status and application of advanced airborne hyperspectral imaging technology: A review. *Infrared Physics & Technology*, 104, Article 103115.
- Joseph, A. O. N. (2012). *Hyperspectral optical imaging for detection, diagnosis and staging of cancer*. University of Southern California.
- Kamandar, M., & Ghassanian, H. (2011). Maximum relevance, minimum redundancy band selection for hyperspectral images. In *2011 19th Iranian conference on electrical engineering* (pp. 1–5). IEEE.
- Karim, S., Qadir, A., Farooq, U., Shakir, M., & Laghari, A. A. (2023). Hyperspectral imaging: a review and trends towards medical imaging. *Current Medical Imaging*, 19(5), 417–427.
- Kaya, G. T., Torun, Y., & Küçük, C. (2014). Recursive feature selection based on non-parallel SVMs and its application to hyperspectral image classification. In *2014 IEEE geoscience and remote sensing symposium* (pp. 3558–3561). IEEE.
- Kennedy, J., & Eberhart, R. (1995). Particle swarm optimization. In *Proceedings of ICNN'95-international conference on neural networks*, vol. 4 (pp. 1942–1948). IEEE.
- Khan, H. A. (2018). *Multispectral constancy for illuminant invariant representation of multispectral images* (Ph.D. thesis), Université Bourgogne Franche-Comté; Norwegian University of Science and ....
- Khan, M. J., Khan, H. S., Yousaf, A., Khurshid, K., & Abbas, A. (2018). Modern trends in hyperspectral image analysis: A review. *IEEE Access*, 6, 14118–14129.
- Khan, H. A., Mihoubi, S., Mathon, B., Thomas, J.-B., & Hardeberg, J. Y. (2018). HyTexiLa: High resolution visible and near infrared hyperspectral texture images. *Sensors*, 18(7), <http://dx.doi.org/10.3390/s18072045>, Retrieved from <https://www.mdpi.com/1424-8220/18/7/2045>.
- Khan, S., Nawaz, M., Guoxia, X., & Yan, H. (2019). Image correspondence with CUR decomposition-based graph completion and matching. *IEEE Transactions on Circuits and Systems for Video Technology*, 30(9), 3054–3067.
- Khan, Z., Shafait, F., & Mian, A. (2013). Hyperspectral imaging for ink mismatch detection. In *2013 12th international conference on document analysis and recognition* (pp. 877–881). IEEE.
- Khan, H. A., Thomas, J. B., & Hardeberg, J. Y. (2017). Multispectral constancy based on spectral adaptation transform. In P. Sharma, & F. M. Bianchi (Eds.), *Image analysis* (pp. 459–470). Cham: Springer International Publishing.
- Khan, H. A., Thomas, J.-B., & Hardeberg, J. Y. (2018). Towards highlight based illuminant estimation in multispectral images. In *International conference on image and signal processing* (pp. 517–525). Springer.
- Khan, H. A., Thomas, J.-B., Hardeberg, J. Y., & Laligant, O. (2017). Illuminant estimation in multispectral imaging. *Journal of the Optical Society of America A*, 34(7), 1085–1098. <http://dx.doi.org/10.1364/JOSAA.34.001085>, Retrieved from <http://opg.optica.org/josaa/abstract.cfm?URI=josaa-34-7-1085>.
- Khan, H. A., Thomas, J.-B., Hardeberg, J. Y., & Laligant, O. (2018). Spectral adaptation transform for multispectral constancy. *Journal of Imaging Science and Technology*, 62(2), 20504–1.
- Khan, H. A., Thomas, J.-B., Hardeberg, J. Y., & Laligant, O. (2019). Multispectral camera as spatio-spectrophotometer under uncontrolled illumination. *Optics Express*, 27(2), 1051–1070. <http://dx.doi.org/10.1364/OE.27.001051>, Retrieved from <http://opg.optica.org/oe/abstract.cfm?URI=oe-27-2-1051>.
- Khan, M. J., Yousaf, A., Abbas, A., & Khurshid, K. (2018). Deep learning for automated forgery detection in hyperspectral document images. *Journal of Electronic Imaging*, 27(5), Article 053001.
- Khaodhia, L., Dinh, T., Schomacker, K. T., Panasyuk, S. V., Freeman, J. E., Lew, R., et al. (2007). The use of medical hyperspectral technology to evaluate microcirculatory changes in diabetic foot ulcers and to predict clinical outcomes. *Diabetes Care*, 30(4), 903–910.
- Kho, E., de Boer, L. L., Van de Vijver, K. K., van Duijnhoven, F., Peeters, M.-J. T. V., Sterenborg, H. J., et al. (2019). Hyperspectral imaging for resection margin assessment during cancer surgery. *Clinical Cancer Research*, 25(12), 3572–3580.
- Khoobehi, B., Beach, J. M., & Kawano, H. (2004). Hyperspectral imaging for measurement of oxygen saturation in the optic nerve head. *Investigative Ophthalmology & Visual Science*, 45(5), 1464–1472.
- Kim, S. J., Zhuo, S., Deng, F., Fu, C.-W., & Brown, M. (2010). Interactive visualization of hyperspectral images of historical documents. *IEEE Transactions on Visualization and Computer Graphics*, 16(6), 1441–1448.
- Kopriva, I., Aralica, G., Hadžija, M. P., Hadžija, M., Dion-Bertrand, L.-I., & Chen, X. (2019). Hyperspectral imaging for intraoperative diagnosis of colon cancer metastasis in a liver. In *Medical imaging 2019: Digital pathology*, vol. 10956 (p. 109560S). International Society for Optics and Photonics.

- Koss, L. G. (1989). The papanicolaou test for cervical cancer detection: a triumph and a tragedy. *Journal of the American Medical Association*, 261(5), 737–743.
- Kothencz, G., Kolcsár, R., Cabrera-Barona, P., & Szilassi, P. (2017). Urban green space perception and its contribution to well-being. *International Journal of Environmental Research and Public Health*, 14(7), 766.
- Kruse, F. A., Lefkoff, A., Boardman, J., Heidebrecht, K., Shapiro, A., Barloon, P., et al. (1993). The spectral image processing system (SIPS)—interactive visualization and analysis of imaging spectrometer data. *Remote Sensing of Environment*, 44(2–3), 145–163.
- Kumar, B., Dikshit, O., Gupta, A., & Singh, M. K. (2020). Feature extraction for hyperspectral image classification: A review. *International Journal of Remote Sensing*, 41(16), 6248–6287.
- Leardi, R. (2001). Genetic algorithms in chemometrics and chemistry: a review. *Journal of Chemometrics*, 15(7), 559–569.
- Lehnert, L. W., Meyer, H., Obermeier, W. A., Silva, B., Regeling, B., & Bendix, J. (2018). Hyperspectral data analysis in R: The hsdar package. arXiv preprint arXiv: 1805.05090.
- Leon, R., Martínez-Vega, B., Fabelo, H., Ortega, S., Melian, V., Castaño, I., et al. (2020). Non-invasive skin cancer diagnosis using hyperspectral imaging for in-situ clinical support. *Journal of Clinical Medicine*, 9(6), 1662.
- Li, Y., Fu, Q., & Heidrich, W. (2021). Multispectral illumination estimation using deep unrolling network. In *Proceedings of the IEEE/CVF international conference on computer vision* (pp. 2672–2681).
- Li, M., Wang, R., & Tang, K. (2013). Combining semi-supervised and active learning for hyperspectral image classification. In *2013 IEEE symposium on computational intelligence and data mining* (pp. 89–94). IEEE.
- Lim, J. K., Li, Q.-X., Ryan, T., Bedgood, P., Metha, A., Vingrys, A. J., et al. (2021). Retinal hyperspectral imaging in the 5xFAD mouse model of Alzheimer's disease. *Scientific Reports*, 11(1), 1–12.
- Liu, L., Catelli, E., Katsaggelos, A., Scutti, G., Mazzeo, R., Milanic, M., et al. (2022). Digital restoration of colour cinematic films using imaging spectroscopy and machine learning. *Scientific Reports*, 12(1), 21982.
- Locherer, M., Hank, T., Danner, M., & Mauser, W. (2015). Retrieval of seasonal leaf area index from simulated EnMAP data through optimized LUT-based inversion of the PROSAIL model. *Remote Sensing*, 7(8), 10321–10346.
- Lodhi, V., Chakravarty, D., & Mitra, P. (2019). Hyperspectral imaging system: Development aspects and recent trends. *Sensing and Imaging*, 20(1), 1–24.
- Lorente, D., Aleixos, N., Gómez-Sanchis, J., Cubero, S., García-Navarrete, O. L., & Blasco, J. (2012). Recent advances and applications of hyperspectral imaging for fruit and vegetable quality assessment. *Food and Bioprocess Technology*, 5(4), 1121–1142.
- Lu, G., & Fei, B. (2014). Medical hyperspectral imaging: a review. *Journal of Biomedical Optics*, 19(1), 010901.
- Lu, G., Halig, L., Wang, D., Chen, Z. G., & Fei, B. (2014). Hyperspectral imaging for cancer surgical margin delineation: registration of hyperspectral and histological images. In *Medical imaging 2014: Image-guided procedures, robotic interventions, and modeling*, vol. 9036 (p. 90360S). International Society for Optics and Photonics.
- Lyngdoh, R. B., Sahadevan, A. S., Ahmad, T., Rathore, P. S., Mishra, M., Gupta, P. K., et al. (2021). AVHYAS: A free and open source QGIS plugin for advanced hyperspectral image analysis. In *2021 International conference on emerging techniques in computational intelligence* (pp. 71–76). IEEE.
- Ma, Z., Li, J., Han, W., Li, Z., Zeng, Q., Menzel, W. P., et al. (2021). Four-dimensional wind fields from geostationary hyperspectral infrared sounder radiance measurements with high temporal resolution. *Geophysical Research Letters*, 48(14), e2021GL093794.
- Manich, C. G., Kelman, T., Coutts, F., Qiu, B., Murray, P., González-Longo, C., et al. (2016). Exploring the use of image processing to survey and quantitatively assess historic buildings. *Structural Analysis of Historical Constructions Anamnesis, Diagnosis, Therapy, Controls*, 125–132.
- Medus, L. D., Saban, M., Francés-Villora, J. V., Bataller-Mompéán, M., & Rosado-Muñoz, A. (2021). Hyperspectral image classification using CNN: Application to industrial food packaging. *Food Control*, 125, Article 107962.
- Melit Devassy, B., & George, S. (2021). Forensic analysis of beverage stains using hyperspectral imaging. *Scientific Reports*, 11(1), 6512.
- Minasny, B., & McBratney, A. B. (2008). Regression rules as a tool for predicting soil properties from infrared reflectance spectroscopy. *Chemometrics and Intelligent Laboratory Systems*, 94(1), 72–79.
- Mirhashemi, A. (2018). Introducing spectral moment features in analyzing the SpecTex hyperspectral texture database. *Machine Vision and Applications*, 29(3), 415–432.
- Mirhashemi, A. (2019). Configuration and registration of multi-camera spectral image database of icon paintings. *Computation*, 7(3), 47.
- Mishra, P., Lohumi, S., Ahmad Khan, H., & Nordon, A. (2020). Close-range hyperspectral imaging of whole plants for digital phenotyping: Recent applications and illumination correction approaches. *Computers and Electronics in Agriculture*, 178, Article 105780. <http://dx.doi.org/10.1016/j.compag.2020.105780>, Retrieved from <https://www.sciencedirect.com/science/article/pii/S016816992031869X>.
- Moharana, S., & Dutta, S. (2016). Spatial variability of chlorophyll and nitrogen content of rice from hyperspectral imagery. *ISPRS Journal of Photogrammetry and Remote Sensing*, 122, 17–29.
- Murphy, J. M., & Maggioni, M. (2018). Unsupervised clustering and active learning of hyperspectral images with nonlinear diffusion. *IEEE Transactions on Geoscience and Remote Sensing*, 57(3), 1829–1845.
- Nagasubramanian, K., Jones, S., Singh, A. K., Sarkar, S., Singh, A., & Ganapathysubramanian, B. (2019). Plant disease identification using explainable 3D deep learning on hyperspectral images. *Plant Methods*, 15(1), 1–10.
- Nawaz, M., Khan, S., Cao, J., Qureshi, R., & Yan, H. (2019). Saliency detection by using blended membership maps of fast fuzzy-c-mean clustering. In *Eleventh international conference on machine vision*, vol. 11041 (pp. 565–572). SPIE.
- Nawaz, M., Khan, S., Qureshi, R., & Yan, H. (2019). Clustering based one-to-one hypergraph matching with a large number of feature points. *Signal Processing: Image Communication*, 74, 289–298.
- Nawaz, M., Qureshi, R., Teevno, M. A., & Shahid, A. R. (2022). Object detection and segmentation by composition of fast fuzzy C-mean clustering based maps. *Journal of Ambient Intelligence and Humanized Computing*, 1–16.
- Nawaz, M., & Yan, H. (2020a). Saliency detection using deep features and affinity-based robust background subtraction. *IEEE Transactions on Multimedia*, 23, 2902–2916.
- Nawaz, M., & Yan, H. (2020b). Saliency detection via multiple-morphological and superpixel based fast fuzzy C-mean clustering network. *Expert Systems with Applications*, 161, Article 113654.
- Nouri, D., Lucas, Y., & Treuillet, S. (2016). Hyperspectral interventional imaging for enhanced tissue visualization and discrimination combining band selection methods. *International Journal of Computer Assisted Radiology and Surgery*, 11, 2185–2197.
- Nouvong, A., Hoogwerf, B., Mohler, E., Davis, B., Tajaddini, A., & Medenilla, E. (2009). Evaluation of diabetic foot ulcer healing with hyperspectral imaging of oxyhemoglobin and deoxyhemoglobin. *Diabetes Care*, 32(11), 2056–2061.
- Olweny, E. O., Faddegon, S., Best, S. L., Jackson, N., Wehner, E. F., Tan, Y. K., et al. (2013). First place: Renal oxygenation during robot-assisted laparoscopic partial nephrectomy: Characterization using laparoscopic digital light processing hyperspectral imaging. *Journal of Endourology*, 27(3), 265–269.
- Oppelt, N., & Mauser, W. (2004). Hyperspectral monitoring of physiological parameters of wheat during a vegetation period using AVIS data. *International Journal of Remote Sensing*, 25(1), 145–159.
- Ortega, S., Halicek, M., Fabelo, H., Guerra, R., Lopez, C., Lejeune, M., et al. (2020). Hyperspectral imaging and deep learning for the detection of breast cancer cells in digitized histological images. In *Medical imaging 2020: Digital pathology*, vol. 11320 (p. 113200V). International Society for Optics and Photonics.
- Osei Darko, P., Kalacska, M., Arroyo-Mora, J. P., & Fagan, M. E. (2021). Spectral complexity of hyperspectral images: a new approach for mangrove classification. *Remote Sensing*, 13(13), 2604.
- Pan, T.-t., Chyngyz, E., Sun, D.-W., Paliwal, J., & Pu, H. (2019). Pathogenetic process monitoring and early detection of pear black spot disease caused by *Alternaria alternata* using hyperspectral imaging. *Postharvest Biology and Technology*, 154, 96–104.
- Paoletti, M., Haut, J., Plaza, J., & Plaza, A. (2019). Deep learning classifiers for hyperspectral imaging: A review. *ISPRS Journal of Photogrammetry and Remote Sensing*, 158, 279–317.
- Peón, J., Recondo, C., Fernández, S., F Calleja, J., De Miguel, E., & Carretero, L. (2017). Prediction of topsoil organic carbon using airborne and satellite hyperspectral imagery. *Remote Sensing*, 9(12), 1211.
- Peyghambari, S., & Zhang, Y. (2021). Hyperspectral remote sensing in lithological mapping, mineral exploration, and environmental geology: an updated review. *Journal of Applied Remote Sensing*, 15(3), 031501.
- Porebski, A., Alimoussa, M., & Vandebroucke, N. (2022). Comparison of color imaging vs. hyperspectral imaging for texture classification. *Pattern Recognition Letters*, 161, 115–121.
- Quemada, M., Gabriel, J. L., & Zarco-Tejada, P. (2014). Airborne hyperspectral images and ground-level optical sensors as assessment tools for maize nitrogen fertilization. *Remote Sensing*, 6(4), 2940–2962.
- Qureshi, R., Uzair, M., Khurshid, K., & Yan, H. (2019). Hyperspectral document image processing: Applications, challenges and future prospects. *Pattern Recognition*, 90, 12–22.
- Qureshi, R., Uzair, M., & Zahra, A. (2020). Current advances in hyperspectral face recognition. TechRxiv.
- Rangnekar, A., Mokashi, N., Ientilucci, E. J., Kanan, C., & Hoffman, M. J. (2020). Aerorit: A new scene for hyperspectral image analysis. *IEEE Transactions on Geoscience and Remote Sensing*, 58(11), 8116–8124.
- Rast, M., & Painter, T. H. (2019). Earth observation imaging spectroscopy for terrestrial systems: An overview of its history, techniques, and applications of its missions. *Surveys in Geophysics*, 40(3), 303–331.
- Ravikanth, L., Jayas, D. S., White, N. D., Fields, P. G., & Sun, D.-W. (2017). Extraction of spectral information from hyperspectral data and application of hyperspectral imaging for food and agricultural products. *Food and Bioprocess Technology*, 10(1), 1–33.
- Reinhard, E., Heidrich, W., Debevec, P., Pattanaik, S., Ward, G., & Myszkowski, K. (2010). *High dynamic range imaging: acquisition, display, and image-based lighting*. Morgan Kaufmann.

- Roy, S. K., Haut, J. M., Paoletti, M. E., Dubey, S. R., & Plaza, A. (2022). Generative adversarial minority oversampling for spectral-spatial hyperspectral image classification. *IEEE Transactions on Geoscience and Remote Sensing*, 60, 1–15. <http://dx.doi.org/10.1109/TGRS.2021.3052048>.
- Roy, S. K., Krishna, G., Dubey, S. R., & Chaudhuri, B. B. (2019). HybridSN: Exploring 3-D-2-D CNN feature hierarchy for hyperspectral image classification. *IEEE Geoscience and Remote Sensing Letters*, 17(2), 277–281.
- Ryu, C., Suguri, M., & Umeda, M. (2011). Multivariate analysis of nitrogen content for rice at the heading stage using reflectance of airborne hyperspectral remote sensing. *Field Crops Research*, 122(3), 214–224.
- Sabzi, S., Pourdarbani, R., Rohban, M. H., García-Mateos, G., Paliwal, J., & Molina-Martínez, J. M. (2021). Early detection of excess nitrogen consumption in cucumber plants using hyperspectral imaging based on hybrid neural networks and the imperialist competitive algorithm. *Agronomy*, 11(3), 575.
- Saeed, N., Murad, M., Nawaz, M., & Irum, M. (2017). Survey on single path and multipath energy efficient routing protocols for wireless sensor networks. *Journal of Computer and Communications*, 5(5), 1–11.
- Saeidan, A., Khojastehpour, M., Golzarian, M. R., Moeenfarid, M., & Khan, H. A. (2021). Detection of foreign materials in cocoa beans by hyperspectral imaging technology. *Food Control*, 129, Article 108242. <http://dx.doi.org/10.1016/j.foodcont.2021.108242>, Retrieved from <https://www.sciencedirect.com/science/article/pii/S0956713521003807>.
- Sagan, V., Maimaitijiang, M., Paheding, S., Bhadra, S., Gosselin, N., Burnette, M., et al. (2021). Data-driven artificial intelligence for calibration of hyperspectral big data. *IEEE Transactions on Geoscience and Remote Sensing*, 60, 1–20.
- Sellami, A., & Tabbone, S. (2022). Deep neural networks-based relevant latent representation learning for hyperspectral image classification. *Pattern Recognition*, 121, Article 108224.
- Shimoni, M., Haelterman, R., & Perneel, C. (2019). Hypersepectral imaging for military and security applications: Combining myriad processing and sensing techniques. *IEEE Geoscience and Remote Sensing Magazine*, 7(2), 101–117.
- Siddiqi, A. M., Li, H., Faruque, F., Williams, W., Lai, K., Hughson, M., et al. (2008). Use of hyperspectral imaging to distinguish normal, precancerous, and cancerous cells. *Cancer Cytopathology: Interdisciplinary International Journal of the American Cancer Society*, 114(1), 13–21.
- Siegmann, B., Jarmer, T., Beyer, F., & Ehlers, M. (2015). The potential of pan-sharpened EnMAP data for the assessment of wheat LAI. *Remote Sensing*, 7(10), 12737–12762.
- Singh, N., Armstrong, D. G., & Lipsky, B. A. (2005). Preventing foot ulcers in patients with diabetes. *Journal of the American Medical Association*, 293(2), 217–228.
- Sokolov, K., Follen, M., & Richards-Kortum, R. (2002). Optical spectroscopy for detection of neoplasia. *Current Opinion in Chemical Biology*, 6(5), 651–658.
- Somedha, C. G. (2017). *Electromagnetic waves*. CRC Press.
- Spectral Color Research Group (2023). *Spectral databases and software: Technical report*, University of Eastern Finland.
- Steinbrener, J., Posch, K., & Leitner, R. (2019). Hyperspectral fruit and vegetable classification using convolutional neural networks. *Computers and Electronics in Agriculture*, 162, 364–372.
- Sun, D.-W. (2010). *Hyperspectral imaging for food quality analysis and control*. Elsevier.
- Sun, W., & Du, Q. (2019). Hyperspectral band selection: A review. *IEEE Geoscience and Remote Sensing Magazine*, 7(2), 118–139.
- Tang, R., Liu, H., Wei, J., & Tang, W. (2020). Supervised learning with convolutional neural networks for hyperspectral visualization. *Remote Sensing Letters*, 11(4), 363–372.
- Thomas, S., Kuska, M. T., Bohnenkamp, D., Brugger, A., Alisaac, E., Wahabzada, M., et al. (2018). Benefits of hyperspectral imaging for plant disease detection and plant protection: a technical perspective. *Journal of Plant Diseases and Protection*, 125(1), 5–20.
- Tilman, D., Balzer, C., Hill, J., & Befort, B. L. (2011). Global food demand and the sustainable intensification of agriculture. *Proceedings of the National Academy of Sciences*, 108(50), 20260–20264.
- Torti, E., Leon, R., La Salvia, M., Florimbi, G., Martinez-Vega, B., Fabelo, H., et al. (2020). Parallel classification pipelines for skin cancer detection exploiting hyperspectral imaging on hybrid systems. *Electronics*, 9(9), 1503.
- Tratt, D. M., Buckland, K. N., Hall, J. L., Keim, E. R., & Johnson, P. D. (2016). Characterization of urban-industrial emissions with airborne thermal-infrared hyperspectral imaging. In *AGU fall meeting abstracts, vol. 2016* (pp. A13N-07).
- Tsai, F., & Philipot, W. (1998). Derivative analysis of hyperspectral data. *Remote Sensing of Environment*, 66(1), 41–51.
- Uzair, M., Mahmood, A., & Mian, A. (2015). Hyperspectral face recognition with spatiotemporal information fusion and PLS regression. *IEEE Transactions on Image Processing*, 24(3), 1127–1137.
- Vali, A., Comai, S., & Matteucci, M. (2020). Deep learning for land use and land cover classification based on hyperspectral and multispectral earth observation data: A review. *Remote Sensing*, 12(15), 2495.
- Vanmeert, F., De Keyser, N., van Loon, A., Klaassen, L., Noble, P., & Janssens, K. (2019). Transmission and reflection mode macroscopic X-ray powder diffraction imaging for the noninvasive visualization of paint degradation in still life paintings by Jan Davidsz. de Heem. *Analytical Chemistry*, 91(11), 7153–7161.
- Vidal, M., & Amigo, J. M. (2012). Pre-processing of hyperspectral images. Essential steps before image analysis. *Chemometrics and Intelligent Laboratory Systems*, 117, 138–148.
- Wan, Y.-q., Fan, Y.-h., & Jin, M.-s. (2021). Application of hyperspectral remote sensing for supplementary investigation of polymetallic deposits in Huanushan ore region, northwestern China. *Scientific Reports*, 11(1), 440.
- Wang, C., Zheng, W., Bu, Y., Chang, S., Zhang, S., & Xu, R. X. (2016). Multi-scale hyperspectral imaging of cervical neoplasia. *Archives of Gynecology and Obstetrics*, 293(6), 1309–1317.
- Weinstein, L. (1988). *Electromagnetic waves*. Moscow: Radio i svyaz'.
- Wood, L. (2022). Global hyperspectral imaging system market 2021 to 2026 rising industrial applications of hyperspectral imaging is driving growth.
- Wyatt, C. (2012). *Radiometric calibration: Theory and methods*. Elsevier.
- Xiao, F., Farrell, J. E., Catrysse, P. B., & Wandell, B. (2009). Mobile imaging: the big challenge of the small pixel. In *Digital photography V*, vol. 7250 (pp. 173–181). SPIE.
- Xing, F., Yao, H., Liu, Y., Dai, X., Brown, R. L., & Bhatnagar, D. (2019). Recent developments and applications of hyperspectral imaging for rapid detection of mycotoxins and mycotoxicogenic fungi in food products. *Critical Reviews in Food Science and Nutrition*, 59(1), 173–180.
- Xiong, Z., Shi, Z., Li, H., Wang, L., Liu, D., & Wu, F. (2017). Hscnn: Cnn-based hyperspectral image recovery from spectrally undersampled projections. In *Proceedings of the IEEE international conference on computer vision workshops* (pp. 518–525).
- Yao, J., Cao, X., Hong, D., Wu, X., Meng, D., Chanussot, J., et al. (2022). Semi-active convolutional neural networks for hyperspectral image classification. *IEEE Transactions on Geoscience and Remote Sensing*, 60, 1–15. <http://dx.doi.org/10.1109/TGRS.2022.3206208>.
- Yasuma, F., Mitsunaga, T., Iso, D., & Nayar, S. K. (2010). Generalized assorted pixel camera: postcapture control of resolution, dynamic range, and spectrum. *IEEE Transactions on Image Processing*, 19(9), 2241–2253.
- Yokoya, N., & Iwasaki, A. (2016). *Airborne hyperspectral data over Chikusei: Technical Report SAL-2016-05-27*, Japan: Space Application Laboratory, University of Tokyo.
- Yusuf, A., & Alawneh, S. (2018). A survey of GPU implementations for hyperspectral image classification in remote sensing. *Canadian Journal of Remote Sensing*, 44(5), 532–550.
- Zeng, M., Cai, Y., Liu, X., Cai, Z., & Li, X. (2019). Spectral-spatial clustering of hyperspectral image based on Laplacian regularized deep subspace clustering. In *IGARSS 2019-2019 IEEE international geoscience and remote sensing symposium* (pp. 2694–2697). IEEE.
- Zhang, L., & Henson, M. J. (2007). A practical algorithm to remove cosmic spikes in Raman imaging data for pharmaceutical applications. *Applied Spectroscopy*, 61(9), 1015–1020.
- Zhang, T., Li, L., & Zheng, B. (2013). Estimation of agricultural soil properties with imaging and laboratory spectroscopy. *Journal of Applied Remote Sensing*, 7(1), Article 073587.
- Zhang, N., Pan, Y., Feng, H., Zhao, X., Yang, X., Ding, C., et al. (2019). Development of fusarium head blight classification index using hyperspectral microscopy images of winter wheat spikelets. *Biosystems Engineering*, 186, 83–99.
- Zhang, J., Su, R., Fu, Q., Ren, W., Heide, F., & Nie, Y. (2022). A survey on computational spectral reconstruction methods from RGB to hyperspectral imaging. *Scientific Reports*, 12(1), 11905.
- Zhang, X., Wen, G., & Dai, W. (2016). A tensor decomposition-based anomaly detection algorithm for hyperspectral image. *IEEE Transactions on Geoscience and Remote Sensing*, 54(10), 5801–5820.
- Zheng, Z., Zhong, Y., Ma, A., & Zhang, L. (2020). FPGA: Fast patch-free global learning framework for fully end-to-end hyperspectral image classification. *IEEE Transactions on Geoscience and Remote Sensing*, 58(8), 5612–5626.
- Zheng, H., Zhou, X., Cheng, T., Yao, X., Tian, Y., Cao, W., et al. (2016). Evaluation of a UAV-based hyperspectral frame camera for monitoring the leaf nitrogen concentration in rice. In *2016 IEEE international geoscience and remote sensing symposium* (pp. 7350–7353). IEEE.
- Zhong, Y., Wang, X., Xu, Y., Wang, S., Jia, T., Hu, X., et al. (2018). Mini-UAV-borne hyperspectral remote sensing: From observation and processing to applications. *IEEE Geoscience and Remote Sensing Magazine*, 6(4), 46–62.
- Zhou, J., & Camba, J. D. (2021). Computer-aided process planning in immersive environments: A critical review. *Computers in Industry*, 133, Article 103547.
- Zuzak, K. J., Naik, S. C., Alexandrakis, G., Hawkins, D., Behbehani, K., & Livingston, E. H. (2007). Characterization of a near-infrared laparoscopic hyperspectral imaging system for minimally invasive surgery. *Analytical Chemistry*, 79(12), 4709–4715.
- Zwinkels, J. (2015). Light, electromagnetic spectrum. *Encyclopedia of Color Science and Technology*, 8071, 1–8.